An Experimental Investigation into the Onset of Smearing Damage in Non-Conformal Contacts with Application to Roller Bearings

Mark Fowell, Stathis Ioannides and Amir Kadiric[*]

Imperial College London, Department of Mechanical Engineering, Tribology Group, SKF UTC for Tribology, London SW7 2AZ, UK

[*]Corresponding author, a.kadiric@imperial.ac.uk

ABSTRACT

The onset of smearing damage was studied under controlled conditions in a custom test rig that simulates the passage of a rolling element through loaded and unloaded zones of a rolling bearing. The set-up comprises a spherical roller which is intermittently loaded between two bearing raceways driven at a prescribed speed. The roller is free to accelerate during the loading phase. Contact load, roller speed and acceleration and electrical contact resistance are recorded during the test. Contact shear stress, friction coefficient, frictional power intensity and elasto-hydrodynamic film thickness are calculated from the recorded kinematics data. Results suggest that the first onset of smearing occurs early in the loading phase where the roller is near-stationary and the frictional power intensity is high. The raceway speed at the onset of damage decreases with increasing load and increasing lubricant supply temperature. The maximum frictional power intensity is found to be relatively constant at all contact conditions that led to

smearing. An existing thermo-mechanical contact model is used to estimate the contact temperature distribution under smearing conditions and the potential for EHL film thickness reduction due to forward heat conduction.

INTRODUCTION

Smearing is a type of surface damage that can occur in rolling bearings if excessive sliding between rolling elements and bearing raceways takes place. This can occur if an element, having lost some of its rotational speed during passage through the unloaded zone, enters the loaded zone of the bearing with surface velocity smaller than that of the contacting raceways. Some typical examples of smearing damage are shown in Figure 1. Smearing scars manifest themselves as plastically sheared regions in the direction of rolling, often accompanied by material removal and deposition as a thin layer on one or both contacting components. This type of damage, associated with high sliding, is broadly similar to scuffing [1, 2], though smearing in rolling element bearings occurs under intermittent loading and transient slide-roll-ratios (SRR) that are determined by contact conditions themselves, unlike scuffing in disc machine tests conducted at fixed SRR, which occurs under steady applied conditions. Since both smearing and scuffing must be preceded by the failure of protective lubricant films under high sliding, similar fundamental mechanisms are likely to be responsible for both.

Smearing is a serious problem in the design of rolling element bearings because it is very difficult to predict and can also be costly due to its tendency to occur in large bearings. For example, smearing has been reported in the intermediate and high speed shaft bearings of wind turbine gearboxes at nominal application speeds. [3].

The literature on smearing in rolling bearings is quite limited. Rowe [4] states that smearing occurs in bearings due to inadequate lubrication and involves transfer of material when the components slide over one another. He notes that smearing most often occurs at the inlet of the loaded zone where the element experiences rapid acceleration. Cocks and Tallian [1] also note that smearing can occur due to deviations in rotational speed of the cage or rolling element from their theoretical speeds or at roller-flange contacts. They draw parallels between smearing and scuffing and present results for onset of smearing with a number of oils in two ball tests under steady sliding conditions. They conclude that the elasto-hydrodynamic (EHL) film plays a major role in determining the load at which smearing occurs. Nelias and co-workers [2, 5] present scuffing results on a twin-disk machine at very high sliding speeds (up to 40m/s) and relatively low loads which were designed to simulate 'skidding' in lightly loaded rolling bearings. The observed damage, involving plastic deformation and material transfer, is representative of instances of smearing in rolling element bearings. The authors provide theoretical predictions of surface and subsurface temperatures for their tests as well as the magnitude of the 'dissipation function' defined as the product of mean fluid shear stress and shear strain rate.

Scherb and Zech [6] provide a detailed study of roller kinematics in cylindrical roller bearings and note the influence of bearing design parameters on the magnitude of sliding between the roller and the rings, with the full complement bearings suffering highest amounts of roller slip. In terms of roller kinematics they identify three zones, a deceleration zone during roller passage

through the unloaded part of the bearing, an acceleration zone at the beginning of the loaded area of the bearing and a constant speed zone that spans the remainder of the loaded area. They conclude that the existence of rolling element slip has a crucial influence on smearing propensity while the bearing load has very little effect. The propensity for smearing is evaluated through the local power of acceleration parameter.

Evans et al [3] used a custom-built experimental rig to create smearing damage in cylindrical roller bearings with different surface treatments. The test conditions leading to smearing were also modelled using a bearing dynamics software and the use of frictional power intensity, defined as $\mu * p_{max} V_s$, as potential smearing criterion was explored with some promising correlations between simulated and test parameters.

Since smearing is initiated at the surface under conditions of increased solid-to-solid contact, it can be intuitively expected that some kind of surface treatment may help in preventing or at least postponing the onset of smearing. Consequently, the effectiveness of various surface treatments has been investigated. The results suggest that diamond like carbon [7], black oxide [6, 8] and tungsten carbide reinforced hydrocarbon [3] coatings can offer significant improvements in this respect over standard bearing surfaces.

Hamer et al [9] studied the conditions leading to onset of smearing using an experimental rig custom-designed to simulate the kinematics of a roller in an operating bearing. A free-rotating spherical roller was repeatedly loaded and unloaded between two bearing raceways driven at a set speed. Smearing damage was successfully reproduced at a range of loads and roller inertias. The authors note that no scuffing was observed if the speed of the roller at the entry to the loaded zone was greater than about 20% of the raceway speed. The collapse of EHL film due to inlet

heating was mentioned as the possible mechanism leading to inset of smearing. An adapted version of the original rig of Hamer and co-workers was also used in the current study and the set-up is described in more detail later in this paper.

In a series of studies, Wadewitz [10], Eglinger [11] and Hambrecht [12] used an experimental set-up similar to that of Hamer et al [9] to study the onset of smearing in rolling-sliding contacts under the loading conditions and contact kinematics closely resembling those found in an operating rolling bearing. Like Hamer et al, their rig consisted of a free rotating roller repeatedly squeezed between two flat discs. The roller in this case was cylindrical and the pulsed load was applied by means of a hydraulic mechanism. The loading mechanism was such that the load profile however was not sinusoidal, as is the case in the current study, but was rising and dropping in a linear fashion during each loading cycle. Wadewitz [10] studied the effects of loading rate, roller inertia and slide-roll ratio. He successfully reproduced smearing damage and subsequently examined a number of criteria in terms of their suitability to predict the onset of smearing and proposed an instantaneous local friction energy criterion as the most suitable. This was defined as:

$$W_r(t) = \int_t^{t+t_{2b}} F_u(\tau) * |V_s(\tau)| \, d\tau \qquad (1)$$

Where $F_u(\tau)$ is the friction force, $V_s(\tau)$ is the sliding speed at time instant t and t_{2b} is the time the roller takes to travel the instantaneous contact width, 2b (τ). Smearing was found to occur when the critical value of W_r, found to lie between 10 mJ and 15 mJ, was exceeded. An alternative parameter equal to the integral of W_r over the roller acceleration phase, with units of Js, was also found to predict the onset of smearing well. Eglinger [11] extended this study by assessing the influence of lubricant viscosity and surface finish on onset of smearing. Although

that study used the same set-up as Wadewitz, the earlier proposed value of critical local friction energy criterion did not predict the onset of smearing well for this set of results, illustrating the difficulty in defining a single parameter for prediction of smearing onset. Finally, Hambrecht [12] used the same set-up to study smearing in grease lubricated contacts.

Unlike smearing in rolling element bearings, scuffing (often termed scoring in the US) has been studied widely, resulting in many proposed scuffing mechanisms. Dyson [13], and more recently Bowman and Stachowiak [14] provide comprehensive reviews of related literature. The earliest scuffing criterion was proposed by Blok [15, 16] who suggested that scuffing occurs when the maximum instantaneous contact temperature reaches some critical value. Given that for scuffing to occur the EHL film must collapse, Dyson and co-workers [17, 18] proposed an alternative criterion of loss of EHL film through heating of lubricant in the contact inlet. They suggested the use of 'frictional power intensity', (defined as $\mu * p * V_s$) as the parameter most suited for prediction of scuffing onset [19]. In another study, accumulation of debris at the contact inlet has also been found to cause EHL film collapse and result in subsequent scuffing [20].

Other authors [21-24] consider desorption of surface boundary films or decomposition of liquid lubricant through polymerisation under elevated temperatures to be prelude to scuffing. At low sliding speeds, where a full EHL film may not be present, these models show promise, but at higher scuffing speeds as well as different rubbing materials the theory is less consistent [14].

It is generally accepted that for scuffing to occur, the macro and micro EHL films as well as any boundary film must collapse. Different lubricated systems will rely on each of these protective lubricant films to a different extent and therefore it is not surprising that no single criterion has proved successful in reliably predicting scuffing in a general lubricated contact.

The current paper presents new results on conditions leading to onset of smearing in concentrated contacts pertinent to rolling bearing conditions. Unlike full bearing tests, the use of a custom experimental rig allows smearing to be studied under controlled conditions so that damage initiation can be observed at an early stage and contact conditions responsible for onset of smearing quantified accurately through analysis of recorded test data. Potential influences of frictional heating are also considered and results discussed in terms of some of the scuffing mechanisms mentioned above.

EXPERIMENTAL SET-UP

This study utilises a custom test rig that was first described in its original form by Hamer at al [9] and has been adapted for the current study. The rig is designed to simulate the passage of a rolling element through the loaded and unloaded zones of an operating rolling bearing. This is achieved by repeatedly pinching a spherical roller between two bearing raceways rotating at a prescribed speed. The basic principle is illustrated in Figure 2, while Figure 3 shows a picture of the complete rig illustrating the specimen arrangement. The two raceways are driven at identical speeds by a 2 HP electric motor. The rotational speed of the raceways can be varied from 0 rpm to 1100 rpm, resulting in raceway surface speeds of 0 m/s to 5.9 m/s. The central spherical roller is not driven and is therefore free to accelerate during the loaded phase due to the torque applied to it through the shear stress generated in the two roller-raceway contacts. Angular speed and acceleration of the roller are monitored via an incremental shaft encoder. Depending on applied load and raceway speed, the roller can experience accelerations of order 10^4 rad/s^2 and in order to monitor such transient kinematics, the encoder position is sampled at a rate of 10 kHz.

The loading is achieved through an eccentrically-mounted, self-aligning ball bearing located on an additional shaft below the lower test ring. This shaft is connected to the ring driving mechanism so that the eccentric bearing acts as a cam pushing on a pivoted cradle which holds the lower ring. The lower ring then loads the central roller, held in its own pivoted cradle, against the upper ring. The pulley arrangement of the driving mechanism is such that the frequency of rotation of the loading shaft, and hence the frequency of applied loading, is half the rotational speed of the two raceways. The magnitude of the load is varied by moving the position of the loading shaft, and hence the eccentric bearing, up and down through a large lever. Once the desired maximum load is achieved the lever can be locked in position. Achievable load range is 0 N to 13.5 kN resulting in contact pressure range of 0 GPa to 3.25 GPa. The load is measured with a load cell mounted at the bottom of the lower cradle and the load cell voltage signal is recorded at frequency of 10 kHz.

The loading mechanism in the experimental set-up is designed to closely re-produce the load profile experienced by rollers in a real roller bearing. The rig load profile resembles a 'clipped sinusoid' and its shape during the loading phase can be expressed as a function of the angular position of the loading cam, ϕ, as $P_r \sim P_{r, max} * (\cos \phi)$. This compares well with the load profile in a real roller bearing where the relationship between the load and the ring angular position takes the form $P_b \sim P_{b, max} (\cos \phi)^{1.1}$, assuming pure radial load and zero clearance [25]. Furthermore, the rig is designed so that the loading cam rotates at half the frequency of the rings, hence the frequency of the test roller loading is half the rotational frequency of driven rings. This simulates the frequency of element loading in large roller bearings, under radial load and inner ring rotation, where the element cage rotates at around half the frequency of the bearing ring [25] so that a given element undergoes loading at every other revolution of the ring. Finally, the range

of loads obtainable in the test rig produces contact pressures between 0 GPa and 3.25 GPa with standard geometry specimens as used in the current study. This covers the complete range of operating pressures encountered in roller bearing contacts, where pressures are limited to below 4 GPa by the bearing static load rating [25] and in most applications bearings operate in the 1 GPa to 2 GPa pressure range.

The main difference between the load experienced by the test roller in the current rig and that seen by a roller in an operating bearing arises from the fact that the test roller is loaded between two identical bearing raceways and subject to the same contact conditions against both raceways. Therefore both roller contacts are identical, with the same level of non-conformity, generally representative of a rolling element – inner ring contact in an operating bearing. In a real bearing, the contact of roller against the outer ring would be considerably different due to a more conformal geometry. However, in a rolling bearing smearing damage most often initiates in the higher pressure contact of rolling element and inner ring [9] and therefore, in respect of smearing onset, the presence of two inner raceway contacts in the current experiment is considered as a reasonable representation of actual bearing contact geometry.

Lubricant is supplied to both contacts through two pressure jets located at the inlet side of both contacts and fed from a central oil tank. The tank incorporates a heating system with a control thermostat so that the oil can be supplied at a desired temperature between ambient and 120 ^{0}C. A 10 μm oil filter is also installed in the closed circuit lubrication system. In the present tests the oil flow rate was 700 ml/sec. It should be noted that, due to the high oil flow rate as well as the size of the tested components, the recorded bulk temperature of the specimens remains largely constant and equal to the oil supply temperature throughout the test, i.e. the tests are isothermal. Although this fact is mainly a side product of the rig design, it simplifies the interpretation of the

results as any influence of the bulk temperature increase is eliminated. The original rig design was adapted during the current project to include a fast roller braking system, a means of monitoring the presence of EHL film and a data acquisition system necessary for detailed monitoring of the highly transient contact conditions.

The current rig design incorporates a magnetic particle brake that can be used to decelerate the test roller during the unloaded zone. Both the brake supply voltage and the application time can be varied, so that the roller speed at the entry to the loaded zone can be set to a desired value. The variable level of external braking simulates different drag forces that may be experienced by the rolling element in a particular bearing size/design due to cage and lubricant drag during roller passage through the unloaded zone of the bearing. The unloaded zone in the current rig is as short as tens of milliseconds, depending on the loading frequencies, so the use of a brake based on magnetic particle technology is necessary in order to apply and release the braking torque within this short period.

An electrical contact resistance measuring system is implemented in the current rig design to provide an indication of EHL film thickness present in the roller-raceway contacts. The roller cradle is electrically insulated from the contacting raceways and a potential difference of 5 V is applied between the roller and the raceways. A high resistance is connected in series to minimise the electrical current in the circuit. The system relies on the fact that an oil film acts as an electrical insulator so that when full EHL film is present in both contacts, the measured potential difference will remain at 5 V. As the oil film decreases the measured potential difference drops significantly and when metal to metal contact occurs, the measured potential can drop to zero. Therefore the recorded voltage signal fluctuates between 5 V and 0 V depending on film conditions within the contacts. The current method provides a relative measure of the present

EHL film and an indication of metal to metal contact, rather than an absolute value of film thickness.

Test Specimens

All test specimens are elements taken from actual roller bearings, so that test surfaces are representative of those found in operation. Raceway specimens are inner raceways from an NU1018 cylindrical roller bearing and the roller specimens are from a 23230 spherical roller bearing. Table 1 lists the geometry and properties of the specimens. The raceway specimens are interference-fitted to custom-made discs before mounting on the test rig and the resulting arrangement can be seen in the photos of Figure 3.

Additive-free PAO 5 base stock is used in the present study with viscosity of 25 cSt at 40° C and 5 cSt at 100° C. Majority of the experiments were conducted at oil supply temperatures of either 17° C or 38° C. A few tests were conducted at higher supply temperatures and these are clearly indicated when relevant results are presented,

Test Procedure

Prior to starting the test, the oil supply is turned on until the surface temperature of the specimens reaches that of the oil supply. The rig is then operated at moderate speed and load for fifteen minutes to run-in the specimen surfaces. The desired load is then applied and the load lever locked in position. The load is held constant during each test. The ring speed is then slowly increased to each desired test value. The test speed increments are 0.25 m/s in the range 1 m/s to

2 m/s, followed by finer increments of as close to 0.1 m/s as the speed control allows from 2 m/s until the speed at which the smearing is detected. The test is run at the particular combination of load and speed for 5 min. If smearing does not occur in the 5 min period the ring speed is then increased to the next desired value. Roller speed, raceway speed, load, electrical contact resistance, oil sump temperature and time stamp are logged on a computer using a custom data acquisition program and are monitored in real time during the test. It should be noted that initially the running time at each condition was longer than 5 min but once it was established that the smearing occurs very quickly, within a few loading cycles once the smearing conditions are reached, the test duration for each set of conditions was set to 5 min. Without detailed tests with real bearings under laboratory conditions, it is rather difficult to relate this observation to the time it takes for smearing to initiate in real bearings. Usually, by the time any damaged bearings have been identified and inspected in a real application the smearing damage would have progressed significantly so that it is not possible to establish the time when the first onset of smearing occurred. However, based on their tests with cylindrical roller bearings, Scherb et al [6] state that smearing only occurred in new bearings and was not observed if the bearing had been running for a while which may offer some evidence that smearing damage also progresses relatively quickly in real bearings.

The test rig is stopped immediately after smearing occurs. The onset of smearing is reliably detected through a marked and sudden increase in noise and vibration as well as an increase in roller maximum acceleration resulting from the increased contact friction. The specimens are then removed and inspected using optical microscopy and surface profilometry.

Over 250 tests were conducted in total. Only the test loads and speeds that actually led to smearing are plotted on the presented graphs.

RESULTS

Kinematics of the Test Roller

Figure 4 illustrates a typical set of load and speed data recorded on the test rig. It can be seen that the test roller enters the loading zone with zero velocity and it is then accelerated, through EHL traction in the two contacts, to the set velocity of the driven raceways. It is this acceleration phase that is potentially damaging to the surfaces due to high sliding velocity and low entrainment speed. The acceleration phase is relatively short and for most of the contact duration the roller velocity equals that of the rings. In the unloaded zone the roller is braked to the desired speed, zero in the example of Figure 4, with the application of the external brake as described above or decelerates due to frictional torque in the support bearings. Such a situation is representative of large slow moving bearings where the unloaded zone lasts long enough for the rolling elements to lose all of their rotational speed due to cage and lubricant drag.

As described in the previous section, the contact load is seen to vary between zero and the maximum, achieved in the centre of the loaded zone, in a manner of a clipped sinusoid. The contact conditions experienced by the specimens are completely transient: the contact pressure distribution, entrainment speed and sliding speed vary continuously throughout each loading cycle.

At higher raceway speeds and higher loads in the current set-up, the duration of the unloaded zone is significantly shortened and, unless the external braking force is applied, the roller does not have sufficient time to lose all of its rotational velocity and so re-enters the loaded zone at non-zero speed, a situation illustrated in Figure 5. This situation is representative of a rolling

bearing where, due to the particular bearing design and operating conditions, the rolling element does not experience sufficient drag forces during passage through the unloaded zone to lose all of its rotational speed.

Figure 6 illustrates a typical set of data obtained at relatively low loads and high sliding speeds, where it is possible that the roller never reaches the speed of the driving raceways. The combination of light load and high speed means that the contact shear stress and in-contact time of the roller are relatively low. Therefore, the torque applied through EHL traction at these conditions is sometimes not sufficient to impart the required impulse to the roller to accelerate it to the speed of the contacting raceways. Such a situation is representative of conditions leading to high speed 'skidding' in bearings. Although the contact pressures are relatively low, these conditions can be damaging as the sliding persists throughout the loaded zone. The range of conditions at which such a situation can occur is obviously very dependent on lubricant properties. A higher viscosity lubricant may help during the loaded zone but would probably cause higher deceleration during the unloaded zone, which would in turn require even higher impulse to be imparted to the roller in the loading phase.

It is worth comparing the contact kinematics achievable on the current rig, as described above, to those experienced in real roller bearings. Scherb et al [6] present measurements of roller speeds in operating roller bearings, obtained using an incremental shaft encoder connected to the rotating roller through a universal joint, for a selection of cylindrical roller bearing designs, bearing speeds and loads. Their data shows the same distinct phases of roller angular acceleration, constant speed and deceleration for all bearing types and speeds studied. Furthermore, for different bearing designs and operating conditions they also observe the variations in the roller angular speed at the entry to the loaded zone, as achievable in the current

set-up (Figures 4 to 6). For example, in a full complement cylindrical roller bearing (SL 192332 C3) loaded with 5 kN the roller will have zero rotational speed at the entry to the loaded zone for bearing speeds below about 480 rpm, whereas at bearing speed of around 800 rpm the roller entering the load zone will still carry about 25% of its maximum rotational speed. For the same bearing loaded with 100kN the roller will have a zero velocity at the entrance to the loaded zone only if bearing speed is below about 160 rpm. Hamer et al [9] and Wadewitz [10] also show equivalent roller speed profiles illustrating the distinct phases of roller acceleration at the entry to the loaded zone, followed by the constant speed of rotation for the remainder of the loaded zone and the roller deceleration phase during the passage through the unloaded zone of the bearing. Therefore, comparison of the roller kinematics obtained in the current rig with the results of existing studies described here confirms that the current experimental set-up is able to reproduce realistic roller bearing contact kinematics.

From the discussion above it is evident that the level of roller deceleration in the unloaded zone of a roller bearing depends on the bearing size, operating conditions and design, particularly the type of element cage. In the current rig, the deceleration of the roller during the unloaded phase, and therefore its velocity at the entry to the loaded zone, can be set to any desired value by the application of a variable braking torque during the unloaded phase. However, the effect of the angular speed of the roller at the entry to the loaded zone on the onset of smearing is not a subject of the present study and consequently, in all tests presented in this paper the roller was braked to zero during the unloaded phase. This condition was chosen as it represents the extreme case in terms of maximum contact slide – roll ratio that may be encountered at rolling element – raceway contact in real rolling bearings and hence is most likely to cause the onset of smearing damage. It therefore helps to define the boundaries of safe contact operation in terms of raceway

speeds, contact loads and lubricant temperatures. From the results of Scherb et al [6] described above it is clear that such extremes of slide-roll ratio do indeed occur in roller bearings. Furthermore, Hamer et al [9] provide a chart in terms of roller bearing pitch diameter and bearing rotational speed to indicate the conditions at which the roller will lose all of its angular speed during the passage through the unloaded zone. For example, they show that a roller in a 0.4 m roller bearing operating at 110 rpm will have zero angular speed at the entrance to the loaded zone. Interestingly, their results suggest that whether or not the roller loses all of its rotational speed is independent of the size of the roller itself.

Conditions Leading to Onset of Smearing

Over of tests were conducted in order to determine safe and unsafe zones of operation in relation to onset of smearing. Figure 7 shows the recorded instances of smearing on the chart of applied maximum contact load P_{max}, against the raceway speed V for two oil supply temperatures, 17° C and 38° C. The conditions at the recorded instances of smearing are also listed in Table 2. Given that the roller speed at the entry to the load zone was zero in all presented cases, the plotted raceway speed is also equal to the maximum sliding speed in any one cycle. A clear pattern is apparent in the data. Conditions that fall above the plotted boundary lines for each test temperature are likely to produce smearing and those below the lines are within the safe operating limits in respect of smearing with the current set-up. The raceway speed at which smearing occurs drops with increasing maximum cycle load but at a relatively slow rate – for an order of magnitude increase in load, the speed only decreases by about 30% at both test temperatures. As may be expected, the load-speed boundary is reached earlier in the tests at the

higher oil supply temperature. For example at a load of 10 kN, the smearing speed for the tests at 17° C is 3.24 m/s compared to 2.6 m/s for the tests at 38° C, an increase in smearing speed of some 20%.

An interesting trend, apparent in both sets of data, is that at very high loads of over 10-11 kN, the smearing speed tends to a constant value of around 3.2 m/s for tests at 17° C and 2.6 m/s for tests at 38° C. Due to the load limitations of the test rig, it was not possible to confirm the existence of this seemingly asymptotic behaviour at higher loads than those already shown in the plots so at present the possible reasons for existence of this limit can only be postulated on. At these high loads the contact pressures are of the order of 3.2 GPa and large parts of the rough contact are likely to be plastic. Any further increase in contact load will therefore not increase the contact pressures significantly. If onset of smearing is related to a critical value of some parameter that is a function of pressure and speed, as is often postulated for scuffing damage, then it may be expected that once the contact pressures reach a relatively constant level, the smearing speed will also remain relatively constant, as observed here, so that the product of load and speed remains at this critical value. However, as mentioned above, this explanation can only be a postulate at the moment and the exact reasons for the observed asymptotic behaviour of smearing speed at high loads are not clear at present.

One of the advantages of the present set-up over smearing studies with full bearings is that the damage can be detected relatively early so that the characteristic features of damaged areas can be observed before they are destroyed by extensive surface failure. Figures 8 and 9 show example pictures, in form of high dynamic range images (HDR), of the smearing damage from two tests listed in Table 2: Test 7 at a high maximum load, $P_{max} = 13.23$ kN, and Test 2 at a relatively low load $P_{max} = 3.14$ kN. As expected, smeared surfaces have a torn appearance due to

extensive metal to metal contact under high sliding leading to plastic deformation at asperity peaks, localised welding and material transfer. A distinctive feature of the smearing marks on the raceway surfaces is their arrow-like shape. This suggests that the damage was initiated early in the loading cycle with the damaged area then widening as the contact area grows under the rapidly increasing load. Identifying the point in the loading cycle when the damage is initiated can help to better understand the mechanisms leading to the onset of smearing.

Figure 10 shows further images of the smeared area on the lower raceway from test 6 which had the maximum contact load of 12.75 kN. It is evident that the extent of damage is not uniform everywhere in the affected area on the raceway. While some areas show clearly torn and dragged surface (Figure 10a), others have relatively light damage (Figure10b). To illustrate this further, Figure 11 shows surface roughness traces taken with a profilometer across the same scars shown in Figure 10. The general area where the traces are taken is shown on the images of Figure 10. The upper roughness trace in Figure 11 shows clear transfer of material and relatively wide damaged area with significantly higher roughness than the surrounding virgin surface. In contrast, the lower trace in Figure 11 shows that the damage in this area of the disc only exhibits some roughening of the surface in the track as compared to the virgin area surrounding it.

Analysis of the recorded kinematic data offers further insight into onset of smearing. From the recorded time histories of contact load and the roller and raceway speeds it is straightforward to calculate the roller acceleration, sliding speed, contact shear stress and instantaneous friction coefficient as functions of time.

Roller angular acceleration is calculated directly from the recorded speed data:

$$\alpha = \frac{d\omega_r}{dt} \tag{2}$$

The mean contact shear stress is given by:

$$\bar{\tau}(t) = 0.5 \frac{I\alpha(t)}{rA(t)} \tag{3}$$

(The factor of 0.5 appears in the Equation 2 to account for the fact that roller is subject to two contacts during loading)

The mean friction coefficient is then:

$$\mu(t) = \frac{\bar{\tau}(t)}{\bar{p}(t)} \tag{4}$$

where the contact area A(t) and mean contact pressure can be calculated for the contact load P(t) using Hertz formulae for elliptical contact.

Finally, the contact instantaneous frictional power intensity (FPI) is given by (note the use of mean pressure in this definition):

$$\ddot{q}(t) = \mu(t) * \bar{p}(t) * V_s(t) \tag{5}$$

Figure 12 shows the time histories of the recorded roller speed, raceway speed, contact pressure, and roller acceleration for 6 loading cycles spanning the onset and subsequent progression of smearing in Test 5 of Table 2. The exact point at which smearing is initiated can be detected by the irregularities in the roller acceleration plot, as indicated in the Figure. Prior to the onset of smearing the roller acceleration traces for each loading cycle have a smooth appearance, due to the fact that the torque is provided purely through the shear stress in the lubricant. The first loading cycle in Figure 12 occurs just prior to the onset of smearing and therefore serves to illustrate the appearance of such smooth acceleration trace prior to the onset of smearing. The second loading cycle in the Figure shows a slight irregularity in the acceleration trace at early

stages of loading. This irregular spike then grows over the next few cycles and by the 6th cycle the acceleration trace clearly contains multiple large spikes. This test was stopped soon after the period shown as the noise and vibration from the rig increased rapidly. The appearance of spikes in the acceleration trace indicates intermittent metal-to-metal contact due to collapse of EHL film. This is accompanied by increased friction and frictional heating, leading to further reduction in EHL film thickness and progressively increasing amounts of metal-to-metal contact, as indicated by appearance of additional spikes in the acceleration trace. Once this situation is reached, surface damage progresses very quickly leading to growth of the smearing scar and increased vibration and noise emanating from the contact.

Figure 13 shows the calculated FPI for the same test but over a longer time span. It is evident that the onset of smearing is also associated with a sudden increase in FPI. Given that the loading and raceway speed do not change over this time period, the rapid rise in frictional heating must have occurred due to the increase in contact friction.

The kinematic data presented in Figure 12 is indicative of tests at relatively high loads, where the first onset of smearing is easily identified and the damage progresses rapidly. The exact loading cycle where smearing initiates is obvious in the recorded data, and smearing is quickly identified during testing through the rapid increase in noise from the test rig. However, at lower loads the damage develops much more slowly and it is not always possible to identify a single loading cycle where the damage is initiated. Instead, the onset of smearing is identified by observation of changes in acceleration and friction coefficient histories over a number of cycles.

It is important to note that the increase in contact friction, frictional power intensity and roller acceleration are a consequence of smearing onset and not the cause of smearing. Therefore, if the

aim is to identify conditions leading to onset of smearing, care must be taken when analysing transient data such as these, to consider the time interval just prior to first initiation of damage rather than immediately after.

Figure 14 shows the data recorded in Test 7 in more detail. The time histories of the load, roller and raceway speeds and contact frictional power intensity are plotted in the lower plot area while the corresponding electrical contact resistance signal and theoretically predicted film thickness are shown in the upper plot area. The film thickness was calculated using the EHL equation of Dowson and Hamrock [26] for elliptical contact, with major axis transverse to direction of rolling and with oil viscosity at the supply temperature of 17°C.

The maximum FPI, 125 MW/m^2 in the Test 7 shown, is reached early during the loading phase. The location of the maximum FPI seems reasonable. In this part of the loading cycle the roller speed is still very close to zero and hence the sliding speed is almost at the maximum; the load is relatively low but so is the contact area and therefore the FPI, as defined in Equation 4, tends to the maximum. As the roller accelerates, the sliding speed diminishes and the frictional heat input rapidly reduces. In test 7 of Figure 14, the roller speed reaches the speed of the raceway at about a fifth of the way into the loaded zone and frictional heating is zero from here on.

The theoretical film thickness is seen to vary in time from minimum right at the beginning of the loaded zone, where the roller is stationary and therefore the entrainment speed is at a cycle minimum, to a maximum when the roller has attained the full speed of the driving raceway. The variation in the applied load has much less influence on the predicted EHD film thickness.

The profile of the ECR signal reflects the general shape of the theoretical film thickness prediction well, but the minimum in ECR seems to occur somewhat later in the loading cycle

than the theoretically predicted minimum film thickness. Furthermore, the trough in the ECR signal also occurs within the period of the elevated frictional power intensity.

Admittedly, the differences in timings of the minimum predicted EHL film thickness and minimum ECR are small and not very obvious from plots such as that in Figure 14, but they are significant since they can only ever be apparent within the very short time period (order of 20 ms) where the acceleration is increasing.

Given that the first onset of smearing (Figure 12) occurs about the same point in the loading cycle where the ECR signal indicates minimum film thickness and the frictional power intensity is near the maximum (Figure 14), it seems sensible to further explore the potential influences of frictional heating.

Frictional Power Intensity

Instantaneous frictional power intensity at all times was calculated for all tests from the roller kinematics data following the procedure outlined previously. The maximum values of FPI, just prior to onset of smearing, were recorded for all combinations of load and speed that led to smearing. The values are listed in Tables 3 and 4, and plotted against raceway speed at smearing in Figures 16 and 17 for the two sets of results obtained at test temperatures of 17 $^{\circ}$ C and 38 $^{\circ}$ C respectively. It is apparent that the maximum FPI at all conditions leading to smearing lie within a relatively narrow range of 105 MW/m^2 to 140 MW/m^2. The significance of the weak trend of slightly increasing FPI with increasing raceway speed, apparent in Figures 16 and 17, cannot be judged without further investigation given the spread in the data. On the other hand, the relative

constancy in FPI seems significant given that the contact loads at which smearing occurred vary by more than an order of magnitude.

The instantaneous contact load and roller speed at which the maximum FPI occurs during the loading cycle were also noted. In all cases FPI reaches the maximum early in the acceleration phase when the roller speed is still very low, 5 to 8% of the raceway speed in all cases. With regards to the load, there appears to be a trend indicating that the greater the maximum cycle load P_{max}, the earlier in the loading cycle the maximum in the FPI is reached. For smearing cases presented in Table 3, the maximum FPI occurs at a load equal to about $0.5*P_{max}$ for the lightest loading case, and at $0.1*P_{max}$ for the heaviest load case. This means that the actual contact pressures and contact areas at the point of maximum FPI differ a lot less between the tests than may be expected given the range of maximum cycle loads studied.

Contact Temperature Predictions

An attempt was also made to estimate the maximum contact temperature and the contact inlet temperature at the contact conditions where the maximum FPI values were recorded. To achieve this, complete surface temperature distributions were predicted using an existing thermo-elastic contact model of Kadiric et al [27]. The model is designed to predict contact pressures, stresses and temperature distributions in a dry, concentrated rough elastic contact of a cylinder sliding on flat. Although this model is designed for steady-state conditions and considers line contacts only, it does predict the complete surface and sub-surface temperature distribution and accounts for variable heat partition fraction directly by matching the temperatures of the two surfaces at all contacting points. It should therefore provide better estimates of contact temperatures for the

current case than the simpler analytical formulas for flash temperatures [28, 29] and, crucially, allows the temperatures at the contact inlet to be noted.

The assumption of steady state heat transfer is an important simplification for the transient contact conditions under consideration. However, in practice steady state is reached after a very short sliding distance, for example, for a square heat source steady state is reached after a sliding distance of only 1.25 * source width [30]. A rough comparison can be made to the present transient contact conditions: the maximum recorded sliding speeds range between 2.6 m/s and 4.75 m/s and the contact width at maximum FPI is around 2b = 600 μm, which means that, under these conditions, the roller slides the distance of 1.25*2b in about 0.3 ms or less. The duration of the sliding zone is of the order of 20 ms (Figures 12 and 14) and therefore near steady state heat transfer conditions should be reached very early into the loaded zone and the steady-state assumption of the applied contact temperature model is a reasonable assumption. Although the model does provide the possibility of including the roughness effects, the present analysis considered smooth surfaces only to help identify general trends in data without additional complications introduced by roughness. The thermo-elastic model is based on dry contact analysis and consequently, when applied to the present case, an assumption is made that all of the generated heat is conducted through the solids and heat convection by the oil is assumed negligible. For thin EHL films, where only a small amount of lubricant flows through the contact, this assumption is generally acceptable. Given that only estimates of contact temperatures are sought and that the ellipticity ratio of the contact in the present tests is over 5, the elliptical contact is modelled in two-dimensions as a contact of a cylinder on a flat in this analysis. The modelled line contact was such that the maximum contact pressure and the contact width in the rolling direction are the same as those recorded for the relevant elliptical contact.

The imposed sliding speed and FPI were those found in the tests. With this approach, the contact

Peclet number ($V_s b/2\kappa$), contact dimensions and the frictional heat intensity are the same as

those recorded in the tests so the obtained temperature estimates are as representative as possible

of the real-life conditions under consideration. Both the sliding speed and the contact load are

considered constant when estimating temperatures with this model. The applied load corresponds

to that recorded in each test at the instant where the FPI is at a maximum. Figure 15 shows an

example of temperature predictions obtained in the way described here for the conditions of Test

2. The shown temperature profile is characteristic of that found for a cylinder in pure sliding on a

stationary smooth half-space [27, 28, 29, 31]. The temperature is seen to peak at a point off the

centre of the contact towards the trailing edge. Inside the contact the roller and the raceway have

the same temperature everywhere since they are in contact. The applied model calculates the

correct local heat partition fraction so that the temperatures of the two contacting bodies are

equal at all points in contact. This is unlike simplified models [28, 29], which only match the

maximum or average temperatures of the two bodies when calculating the heat partition fraction.

Outside the contact area, the raceway, which is moving with respect to the contact, is cooler than

the roller and its temperature falls to the bulk temperature very quickly at the leading edge. On

the other hand, the surface temperature of the roller, which is stationary relative to the contact, is

higher than bulk at the leading edge. It is this roller surface temperature at the inlet that is

important when determining the correct viscosity of the lubricant in the film thickness

calculations that include inlet heating. The roller temperature is seen to fall slightly at the first

point in contact with the disc on the inlet side. Such a roller temperature profile occurs because

in steady state heat transfer, the stationary roller gets hotter than the raceway which is moving

with respect to the contact. The moving raceway presents cooler material as it comes into contact

with the hotter roller and at the instant of first contact a point on the raceway has to

instantaneously reach the temperature of the hotter roller. For this to occur there must be some

heat conduction from the roller to the raceway and effective local heat partition fraction is

greater than 1. The behaviour described here has been predicted by other authors [27, 31] and the

reader is referred to these works for further details.

More accurate predictions could be obtained by using a full thermal EHL model, accounting for

presence of lubricant and particularly its effect on heat partitioning as done by Evans et al [32],

but such a treatment is beyond the scope of the current paper.

Table 3 and Table 4 list the values of the estimated maximum contact temperatures, contact inlet

temperatures (taken at a point 0.1b ahead of the contact) and the maximum frictional heat

intensity for all conditions under which smearing was observed in the two sets of results for oil

supply temperatures of 17° C and 38° C respectively. Figures 16 and 17 plot these temperatures

against the raceway speed at smearing directly above the PV chart of the corresponding smearing

points for the two sets of results at 17° C and 38° C respectively. From Table 3 and Figure 16, it

is evident that at the oil supply temperature of $17^{°}$ C, the estimated maximum contact

temperatures lie in the range of $157^{°}$C to $191^{°}$C and the inlet temperatures between $59^{°}$ C and $69^{°}$

C. From Table 4 and Figure 17, the corresponding ranges for the tests conducted at oil supply

temperature of 38° C are $180^{°}$ C to $206^{°}$ C and $82^{°}$ C to $92^{°}$ C.

Film Thickness Predictions

Minimum film thicknesses at all points during the loading cycle were predicted with standard

EHL equations [26] using the recorded contact load and entrainment speed time histories. Given

the presence of dynamic loading, the contribution of any squeeze films was also considered. The

squeeze film would act to increase the minimum film thickness during the loading phase, where

the contact width in the rolling direction is increasing with time, and to decrease the minimum

film during the unloading zone where the contact width is shrinking. From the recorded loading

histories the rate of growth of contact width, db/dt, was calculated at all times. It was found that

the maximum db/dt is of the order of 10^{-4} m/s and occurs at the point where the contact pressure

is about 10% of the maximum value. It is estimated that this expansion/contraction of the contact

size results in about 5% increase in film thickness during loading phase and about 2 to 3%

reduction during the unloaded phase. (It should also be noted that the EHL film thickness is

relatively high during the unloading phase as the entrainment speed here is the highest). Given

these small magnitudes of the squeeze films, they were neglected in all theoretical film thickness

predictions.

Tables 3 and 4 list the values of the cycle minimum film thickness at smearing conditions

obtained with straightforward application of Dowson and Hamrock equation [26] with the

viscosity of lubricant at the oil supply temperature. The predicted films range between 370 nm

and 500 nm for the test conducted at $17^{°}$ C, and between 176 nm and 220 nm for the tests at $38^{°}$

C. Compound R_q value for the two specimens is around 105 nm and therefore this isothermal

analysis predicts λ values in the range of 1.7 to 4.7 at conditions leading to smearing over the

whole range of loads, speeds and temperatures tested. If it is accepted that the collapse of the

macro EHL film is a necessary, if not a sufficient, condition for scuffing to occur, it would seem

unlikely that the theoretical isothermal film thickness values as calculated here are representative of the actual film at smearing. Consequently, film thicknesses were re-calculated using the oil viscosity at the estimated inlet temperatures listed in Tables 3 and 4, instead of the oil supply temperature. These reduced film thickness values are listed in the last column of Tables 3 and 4. They range from 63 nm to 174 nm over the whole range of conditions where smearing occurred, which corresponds to λ values of about 0.6 to 1.6. Thus, the reduced film thickness values seem a much more reasonable estimate of what may be expected at the onset of smearing where some metal-to-metal contact must be occurring.

Effect of Lubricant Supply Temperature

To further investigate the effects of lubricant temperature, additional tests were conducted at constant load of 12.75 kN (p_0 = 3.2 GPa) but varying lubricant supply temperature. Prior to starting each test at elevated temperature, the oil supply was turned on and the oil was allowed to flow over the specimens until the specimen bulk temperature reached that of the oil supply. Table 5 lists the relevant values of maximum contact load and raceway speed at smearing, along with FPI, maximum contact temperatures and inlet temperatures, all calculated in the same manner as in the previous section. Figure 18 plots this data on the graph of raceway speed at the onset of smearing against oil supply temperature. It is evident that the raceway speed at smearing decreases with increasing lubricant temperature relatively rapidly, from 3.21 m/s at 17°C down to 1.8 m/s at 80 $^{\circ}$C, i.e. a drop of just under 50%. For comparison, in the tests at 17°C presented in the previous section, for an increase in load of an order of magnitude, the raceway speed at smearing dropped by just over 30%.

DISCUSSION

The observed trend of decreasing sliding speed at smearing with increasing maximum cycle load is in line with many reported scuffing results [1, 13, 14]. Comparison of the precise shape of the observed load-speed curves with scuffing studies is rather difficult because the loading in the current tests is intermittent while sliding speeds are transient and internally generated rather than externally imposed. The properties of the lubricant used will also have a profound effect.

It is, however, interesting to discuss the present findings in relation to suggested mechanisms of scuffing. In this respect, the observed trend in maximum instantaneous frictional power intensity (FPI) seems significant. In all recorded occurrences of smearing the maximum value of FPI lies in the relatively narrow range of 105 MW/m^2 to 140 MW/m^2, despite the fact the load varies by an order of magnitude. The FPI has been considered as a scuffing criterion by Bell and Dyson [19] amongst others and has also been considered as a potential smearing criterion [3, 10]. Theoretically-predicted maximum contact temperatures, assuming smooth surfaces, vary between 157°C and 206°C at onset of smearing in this study for oil supply temperatures of 17° C or 38° C. Contact temperatures of the order of 150°C have been previously suggested as the transition point leading to scuffing damage for additive-free mineral oils [33] but predictions vary significantly for different lubricated systems and can range from 150 $^{\circ}$C to over 400 $^{\circ}$C [14]. Other authors [6] have used maximum frictional power as the smearing criterion but this parameter was found to vary significantly at conditions leading to onset of damage in current tests, having values between 125W and 290W.

To accurately describe transient conditions in the present study a large amount of data needs to be recorded and analysed, but this does help reveal other information about damage initiation. The maximum FPI in the current studies occurs early in the loading cycle (Figure 14) when the roller is still close to stationary. Under such conditions, significant forward heat conduction to the inlet can occur through the stationary roller. (On the other hand, the raceway, which is moving at high speed relative to the contact, does not contribute significantly to the inlet heating). Furthermore, the contact width at the point where FPI is maximum is comparatively small, which will further increase the inlet temperature as the inlet is closer to the centre of the contact. Given the magnitudes of FPI and the contact conditions when they occur, contact inlet temperatures of between 60 $^{\circ}$C and 90 $^{\circ}$C have been estimated at the onset of smearing for test temperatures of 17°C or 38°C, as shown in Tables 3 and 4. As a result of this inlet heating, the lubricant specific film thickness was predicted to drop to $0.6 \leq \lambda \leq 1.6$ from the isothermal value of $1.7 \leq \lambda \leq 4.7$. These reduced film thicknesses seem to be reasonable estimates for conditions at onset of smearing. Given that an additive-free oil was used in the present testing, surface damage initiation would certainly be possible with such thin EHL films; for example, the critical film thickness for gears has been found to be $0.5 \leq \lambda \leq 1.7$ [14] which encompasses the range of reduced films predicted here. The ECR signal in Figure 14 also indicates that the film thickness is at a minimum in the same general region of the loading cycle where FPI is near its maximum, while the appearance of spikes in the acceleration trace shows that the onset of metal to metal contact occurs in the same general region. Further analysis is needed to confirm the exact processes taking place during this rapid acceleration phase in the loading cycle, but it can be tentatively suggested that the combination of high FPI and near-stationary roller can lead to considerable inlet heating, causing a subsequent drop in lubricant viscosity to a level where the

protective EHL film is reduced sufficiently to cause initial metal-to-metal contact. Once this situation is reached, the contact friction and consequently the frictional heating will increase further (Figure 13), leading to an increasing drop in EHL film thickness and spreading metal-to-metal contact, as indicated by appearance of extra spikes in the acceleration trace in Figure 12. This self-enforcing mechanism fairly quickly results in significant surface damage. The mechanism of contact inlet temperature rise as a prelude to scuffing has been considered by other authors, notably Dyson and co workers [17, 18], while Hamer et al [9] also suggests its apparent importance in onset of smearing in rolling bearings.

However, the onset of smearing is likely a product of multiple mechanisms and further studies are needed to fully understand the processes leading to damage initiation. The present investigation does not consider a number of important factors including the role of micro EHL films, non-zero roller velocity at the entry to the loaded zone or the effects of surface roughness, other than through general λ ratio. Furthermore, all tests in the current study were performed with a single lubricant, same specimen material and relatively consistent surface roughness textures so it is difficult to extrapolate the present observations to other lubricated systems. It is also unclear if the simultaneously transient loads, speeds and accelerations affect the onset of damage in ways not encountered in steady state scuffing tests. Additional tests are currently being conducted in an attempt to answer some of these questions.

CONLCUSION

Smearing damage has been successfully created under controlled conditions in a custom test rig. The recorded kinematics of the test roller were representative of those found in a rolling bearing

which is experiencing roller slowdown in the unloaded zone and roller slip in the loaded zone of the bearing.

At the studied contact conditions with additive free PAO5 oil and constant lubricant supply temperature of 17° C, the raceway speed at which smearing occurred decreased by about 30% (from 4.75 m/s to 3.2 m/s) for an order of magnitude increase in maximum cycle load (from 1.2 kN to 13.2 kN, equivalent Hertz pressure range of 1.4 GPa to 3.23 GPa). At lubricant supply temperature of 38° C the corresponding decrease in smearing speed was also 30% (from 3.75 m/s to 2.6 m/s), for the load range of 2 kN to 12.75 kN. In tests at constant maximum load of 12.75 kN (Hertz pressure of 3.2 GPa) the raceway speed at smearing reduced from 3.2 m/s to 1.8 m/s for the increase in lubricant supply temperature from 17° C to 80° C.

The first onset of metal-to-metal contact is manifest as the appearance of spikes in the roller acceleration trace and an increase in contact friction and frictional power intensity. The recorded data indicate that the first metal-to-metal contact occurs in the early stages of the loading cycle where the roller is almost stationary. The frictional power intensity was found to peak in the same region of the loading cycle while the electrical contact resistance signal indicates that the minimum EHL film thickness also occurs in this part of the cycle.

The maximum in mean frictional power intensity during the loading cycle was found to be relatively constant at the observed instances of smearing onset, lying in the range between 105 MW/m^2 and 140 MW/m^2 for all loads and speeds at which smearing occurred for oil supply temperatures of 17° C or 38°C. Theoretical predictions of contact temperature distributions suggest that significant heating of contact inlet can occur at contact conditions that led to damage initiation where the test roller is stationary prior to entering the loaded zone. Predictions of EHL

film thickness indicate that the inlet temperature rise at the onset of smearing may lead to a drop in specific EHL film thickness from $1.7 \leq \lambda \leq 4.7$ across all loads and speeds where smearing occurred and with the viscosity of oil at the test supply temperatures (17° or 38°C), to $0.6 \leq \lambda \leq 1.6$ with the viscosity at the estimated inlet temperatures in the same tests. Further tests are ongoing to gain further understanding of the multiple mechanisms that are likely to be responsible for onset of smearing damage.

ACKNOWLEDGEMENTS

REFERENCES

1. Cocks, M. and Tallian, T. E. (1971), "Sliding contacts in rolling bearings," ASLE Trans. 14, pp. 32-40.

2. Nelias, D., Nasarre, F. and Flamand, L. (1995), "Scuffing at very high sliding speed and low normal load: an experimental investigation," Proceedings of the International Tribology Conference, Yokohama, Japan.

3. Evans, R. D., Barr, T. A., Houpert, L. and Boyd, S.V. (2013), "Prevention of smearing damage in cylindrical roller bearings", STLE Tribol. Trans., Accepted Manuscript, March 2013, DOI: 10.1080/10402004.2013.788236

4. Rowe, F. D. (1971), "Diagnosis of rolling contact bearing damage," Tribology 4, pp. 137-149.

5. Nelias, D. (1997), "Etude experimentale et theorique du micro grippage dans les contacts elastohydrodynamiques," Rev. Gen. Therm. 36, pp. 26-39 (in French).

6. Scherb, B. J. and Zech, J. (2001), "A study on the smearing and slip behavior of radial cylindrical roller bearings," Georg Simon Ohm Series, University of Applied Sciences Nuremberg, ISSN 1616-0726.

7. Pihlstrom, L. and Strom, E. (1998), "Smearing protection and smearing physics," Master Thesis GT98D029, Chalmers University of Technology, Goteborg, Sweden.

8. Miailidis, A., Salpistis, C., Panagiotidis, K., Sachanas, C., Gatsios, S., Hoffinger, C. and Bakolas,V. (2010), "Wear and smearing resistance of black iron mixed oxide coated steels," Int. J. Surf.Sci. and Engr. 4, 4/5/6, pp. 337-359.

9. Hamer, J. C., Sayles, R. S. and Ioannides, E. (1991), "An experimental investigation into the boundaries of smearing failure in roller bearings," ASME J. Tribol. 113, pp. 102-109.

10. Wadewitz, M. (1993), "Anschmierungserscheinungen: Ursachen der anschmierungen im Waltz-/Gloetkontakt", Doctoral Thesis, 1993:Forschungsvorhaben Nr. 164/I, Universitat Erlangen-Nurnberg, Erlangen, Germany (in German)

11. Eglinger, M. (1995), "Anschmierungserscheinungen: Einflus des smierstoffes und der Rollenbeschaffenheit auf die Entstehung von anschmierungen", Doctoral Thesis, 1995:Forschungsvorhaben Nr. 164/II, Universitat Erlangen-Nurnberg, Erlangen, Germany (in German)

12. Hambrecht, R. (1999), "Anschmierungserscheinungen in walzlagern bei fettschmierung", Doctoral Thesis, 1999: Nr. 321, Universitat Erlangen-Nurnberg, Erlangen, Germany (in German)

13. Dyson, A. (1975), "Scuffing – a review," Tribol. Intl. 8, 2, pp. 77-87.

14. Bowman, W.F. and Stachowiak, G.W. (1996), "A review of scuffing models." Tribology Letters 2, pp. 113-131.

15. Blok, H. (1939), "Seizure delay method for determining the protection against scuffing afforded by extreme pressure lubricants," J. Society of Auto Engrs 44, 5, pp. 193-210.

16. Blok, H. (1969), "A postulate about the constancy of scoring temperature," Interdisciplinary Approach to the Lubrication of Concentrated Contacts, Publ. NASA, Washington DC, SP-237, pp. 153-224.

17. Dyson, A. (1976), "The Failure of Elastohydrodynamic Lubrication of Circumferentially Ground Discs," Proc. Inst. Mech. Engnrs. 190, pp. 52-76.

18. Cheng, H.S. and Dyson, A. (1978), "Elastohydrodynamic Lubrication of Circumferentially Ground Rough Disks," Trans. ASLE 21, 1, pp. 25-40.

19. Bell, J.C. and Dyson, A. (1972), "The effect of some operating variables on the scuffing of hardened discs," Proc. I. Mech. E. Symp. on EHL, 186, C11/72, pp. 61-67.

20. Enthoven, J. and Spikes, H.A. (1996), "Infrared and Visual Study of the Mechanisms of Scuffing," Trib. Trans. 39, pp. 441-447.

21. Spikes, H. A. and Cameron, A. (1974), "Scuffing as a desorption process - explanation of borsoff effect," ASLE Trans. 17, pp. 92-96.

22. Lee, S.C. and Cheng, H. S. (1991), "Scuffing Theory Modelling and Experimental Correlations," ASME J. Tribol. 113, 2, pp. 327-334.

23. Lee, S.C and Cheng, H. (1995), "Experimental validation of critical temperature-pressure theory of scuffing," Tribol. Trans. 38, 3, pp. 738-742.

24. S.M. Hsu, M.C. Shen, E.E. Klaus, H.S. Cheng, P.I. Lacey (1994), "Mechano-chemical model: reaction temperatures in a concentrated contact", Wear, 175, pp. 209-218.

25. Harris, T. (2001), "Rolling bearing analysis", 4th Edition, Wiley, 2001

26. Hamrock, B. J. and Dowson, D. (1981), "Ball Bearing Lubrication", John Wiley and Sons, London, UK

27. Kadiric, A., Sayles, R. S. and Ioannides, E. (2008), "Thermo-mechanical model for moving layered rough surface contacts", Journal of Tribology 130, 1, pp. 011016(1-14).

28. Jaeger, J. C. (1942), "Moving sources of heat and the temperature at sliding contacts", Proc. R. Soc N. S. W., 76, pp. 203-224.

29. Blok, H. (1937), "Theoretical study of temperature rise at surface of actual contact under oiliness lubricating conditions", Instn. Mech. Engrs., Proceedings of General Discussion on Lubrication and Lubricants, 2, pp. 222-235

30. Bhushan, B. (1999), "Principles and Applications of Tribology", John Wiley & Sons, New York, US

31. Bos, J and Moes, H. (1995), "Frictional heating of tribological contacts", ASME Journal of Tribology 117, pp. 171-177

32. Evans, H. P., Clarke, A., Sharif, K. J. and Snidle, R. W. (2010), "The Role of Heat Partition in Elastohydrodynamic Lubrication," Tribol. Trans. 53, 2, pp. 179-188

33. Kelly, B. V. (1953), "A new look at the scoring phenomena of gears," SAE Trans. 61, pp 175-188.

NOMENCLATURE

A, Contact area (m^2)

E, Young's modulus (GPa)

I, Mass moment of inertia of the test roller (kg/m^2)

P, Load (kN)

P_{max}, Maximum load in a loading cycle (kN)

R_q, Root-Mean-Square roughness (m)

T_i , Contact inlet temperature at 1.1b (^0C)

T_{max}, Maximum contact temperature (^0C)

T_{sup}, Temperature of oil supply (^0C)

V_s, Sliding speed (m/s)

V, Velocity of the raceway surface (m/s)

b, semi-minor axis of the contact (m)

c_p, Specific heat capacity (J/kgK)

h_o, Minimum film thickness (nm)

k, Thermal conductivity (W/mK)

p, Contact pressure (GPa)

p_0, Hertz maximum pressure

$\ddot{q}$, Frictional power intensity (MW/m^2)

r, radius of the test roller (m)

t, time (s)

α, Angular acceleration of the test roller (krad/s^2)

κ, Diffusivity (=k/ρc_p) (m^2/s)

λ, Specific film thickness (=h_o / R_q)

μ, Friction coefficient

ρ, Density (kg/m^3)

τ, Contact shear stress (Pa)

υ, Poisson's ratio

ω_r, Angular velocity of the test roller (rad/s)

TABLES

Table 1: Properties of test specimens

	Raceways	**Spherical Roller**
Geometry	$R_x = 51.5$ mm, $R_y = \infty$	$R_x = 15$ mm, $R_y = 124$ mm
Material	AISI 52100 Steel	AISI 52100 Steel
Elastic properties	$E = 210$ GPa, $\upsilon = 0.3$ Hardness = 60 HRC	$E = 210$ GPa, $\upsilon = 0.3$ Hardness = 60 HRC
Thermal properties	$k = 45$ W/mK, $\rho = 7860$ kg/m^3, $c_p = 460$ J/kgK	$k = 45$ W/mK, $\rho = 7860$ kg/m^3, $c_p = 460$ J/kgK
Surface roughness	$R_q = 95$ nm	$R_q = 45$ nm

Table 2: Maximum applied load and raceway speed at which onset of smearing was recorded at test temperatures of 17° C and 38° C.

Test No#	P_{max} (kN)	V (m/s)	Test Temperature (°C)
1	1.20	4.75	17
2	3.14	4.53	17
3	5.10	4.2	17
4	6.56	3.57	17
5	9.78	3.24	17
6	12.75	3.21	17
7	13.23	3.22	17
8	12.75	2.58	38
9	11.50	2.60	38
10	11.14	2.60	38
11	10.00	2.68	38
12	6.42	3.18	38
13	3.90	3.30	38
14	2.00	3.75	38

Table 3: List of maximum frictional power intensity (FPI), predicted maximum contact temperature (T_{max}), predicted inlet temperature (T_i), predicted cycle minimum film thickness (h_o) at oil supply temperature and reduced minimum film thickness at inlet temperature, for all contact conditions that led to onset of smearing in tests at oil supply temperature (and bulk temperature) equal to 17° C.

Test No#	P_{max} (kN)	V (m/s)	$\ddot{q}$ (MW/m^2)	T_{max} (^{0}C)	T_i (at 1.1b) (^{0}C)	h_o (isothermal prediction) (nm)	Reduced h_o (prediction with inlet heating) (nm)
1	1.20	4.75	140	157	59	498	174
2	3.14	4.53	130	166	61	454	140
3	5.10	4.2	130	176	64	431	129
4	6.56	3.57	125	191	69	390	125
5	9.78	3.24	118	175	65	370	106
6	12.75	3.21	113	174	64	396	114
7	13.23	3.22	125	165	62	370	111

Table 4: List of maximum frictional power intensity (FPI), predicted maximum contact temperature (T_{max}), predicted inlet temperature (T_i), predicted cycle minimum film thickness (h_o) at oil supply temperature and reduced minimum film thickness at inlet temperature, for all contact conditions that led to onset of smearing in tests at oil supply temperature (and bulk temperature) equal to 38° C.**Test No#**

Test NO#	P_{max} (kN)	V (m/s)	$\ddot{q}$ (MW/m^2)	T_{max} (^{0}C)	T_i (at 1.1b) (^{0}C)	h_o (isothermal prediction) (nm)	Reduced h_o (prediction with inlet heating) (nm)
8	12.75	2.58	110	189	85	176	69
9	11.50	2.60	115	198	90	179	65
10	11.14	2.60	130	206	92	179	63
11	10.00	2.68	105	182	84	181	72
12	6.42	3.18	117	180	82	198	81
13	3.90	3.30	113	181	84	203	81
14	2.00	3.75	126	191	84	220	87

Table 5: List of maximum frictional power intensity (FPI), predicted maximum contact temperature (T_{max}), predicted inlet temperature (T_i), predicted cycle minimum film thickness (h_o) at oil supply temperature and reduced minimum film thickness at inlet temperature, for all disc speeds that led to smearing in tests conducted at the same maximum contact load of 12.76 kN (P_0 = 3.2 GPa) at five different oil supply temperatures.

Test No#	Oil Supply Temp. (^{0}C)	V (m/s)	$\ddot{q}$ (MW/m^2)	T_{max} (^{0}C)	T_i (at 1.1b) (^{0}C)	h_o (isothermal prediction) (nm)	Reduced h_o (prediction with inlet heating) (nm)
15	17	3.21	113	174	64	396	114
16	22	3	115	182	71	326	100
17	38	2.58	110	189	85	176	69
18	60	2.1	112	232	117	91	42
19	80	1.8	115	286	147	62	29
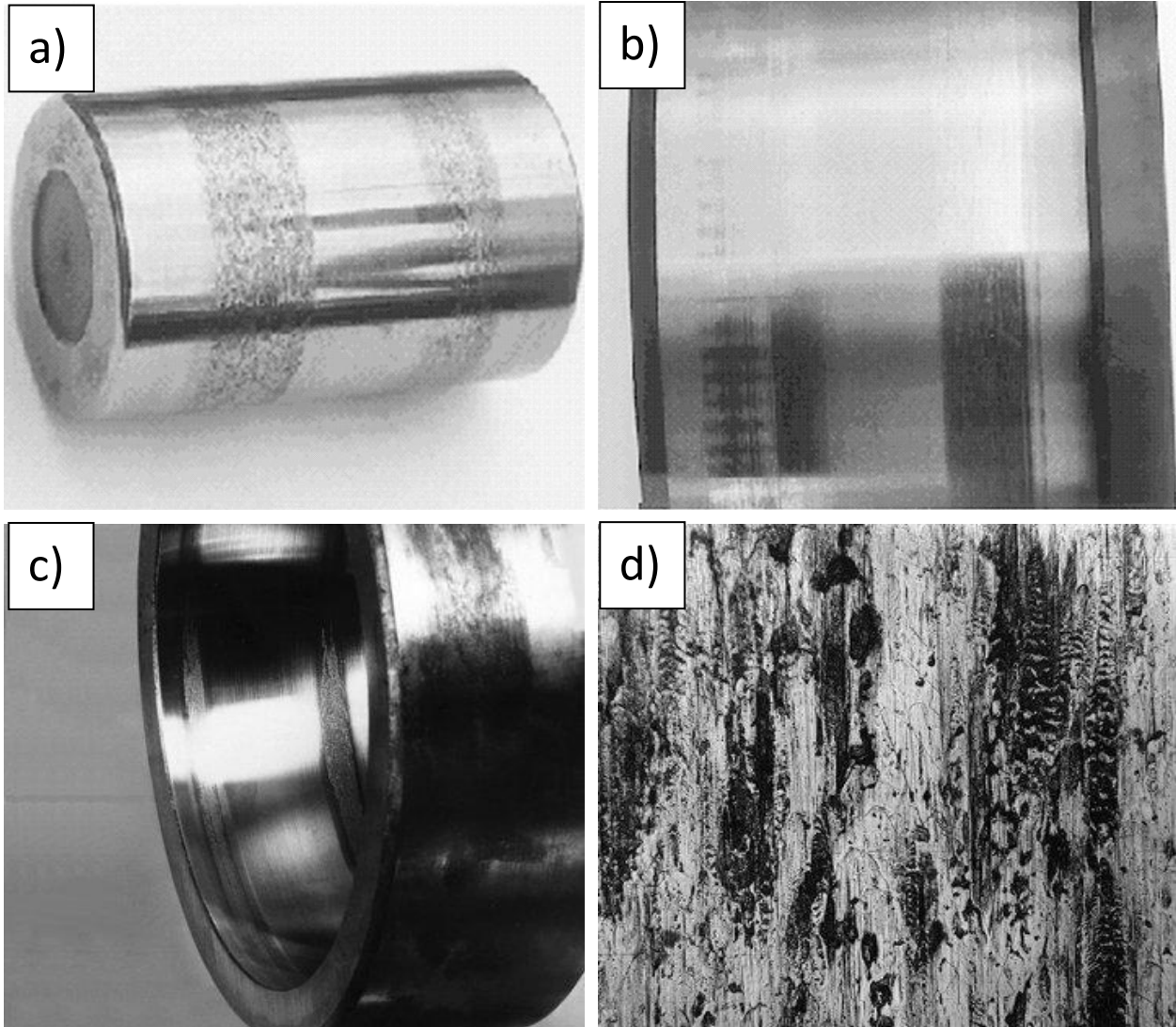
Figure 1: Examples of smearing damage in rolling bearings: a) smeared roller from a cylindrical roller bearing (CRB) [6]; b) smearing damage on the inner ring of a CRB [6]; c) Smearing damage on both outer raceways of a spherical roller bearing (SRB) d) Smeared area on a spherical roller from an SRB (www.skf.com)
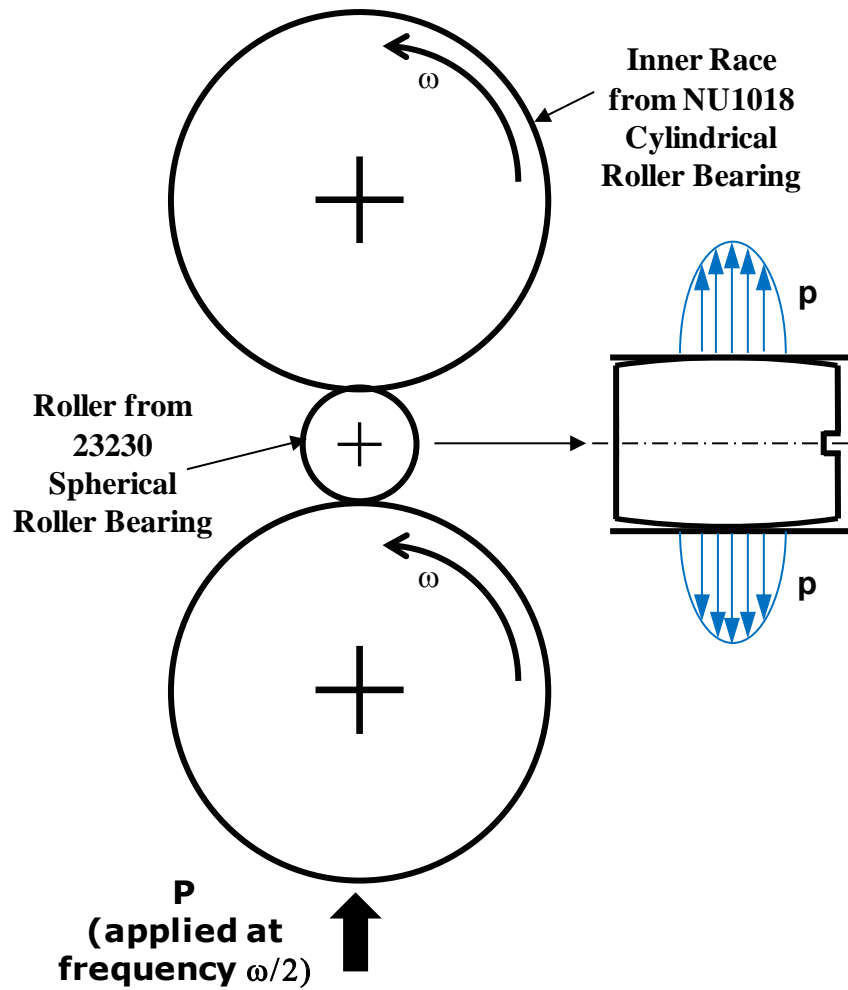
Figure 2: Schematic of the experimental rig set-up which simulates a rolling element travelling through loaded and unloaded zones of an operating bearing: The central spherical roller is repeatedly loaded between the two raceways which are driven at a constant speed. The roller is free to accelerate during the loaded phase and decelerates during the unloaded phase either due to an applied braking torque or losses in support bearings. (Not to scale)
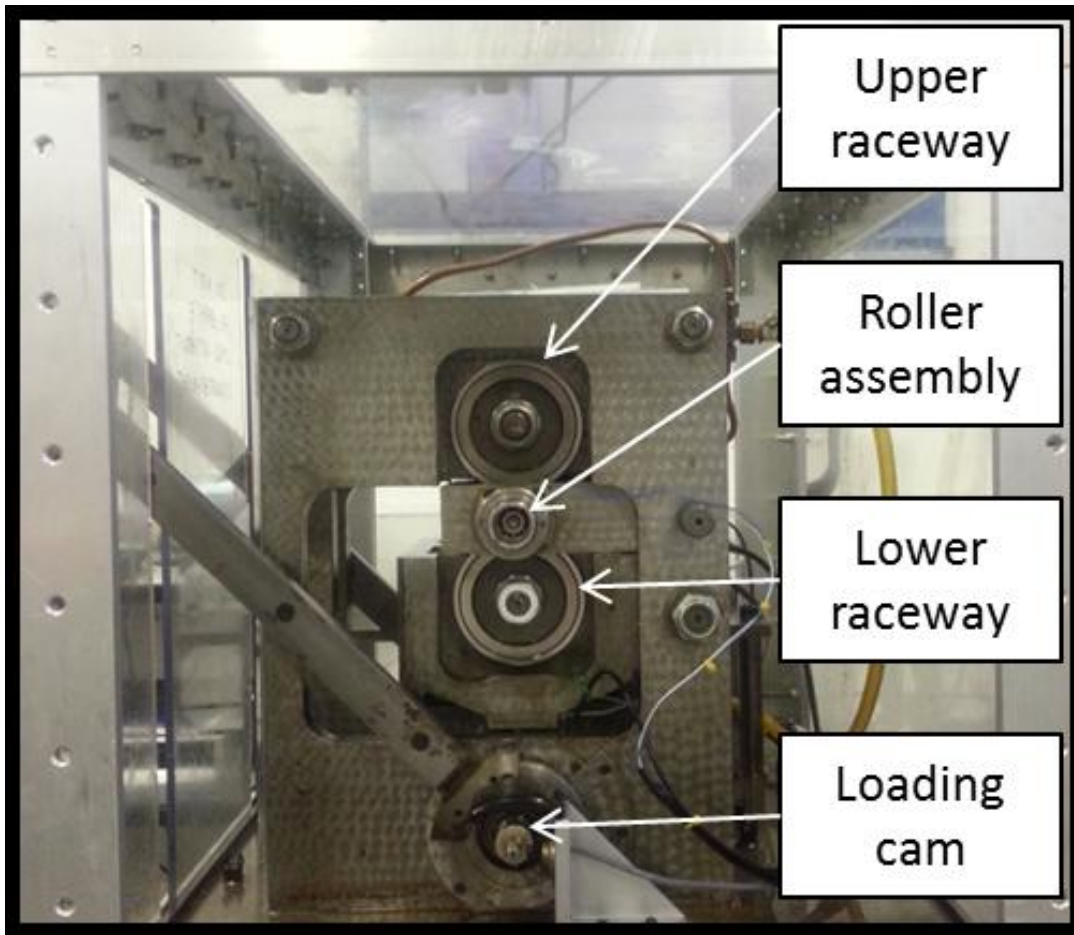
Figure 3: Front view of the smearing test rig showing the three specimens and the loading cam.
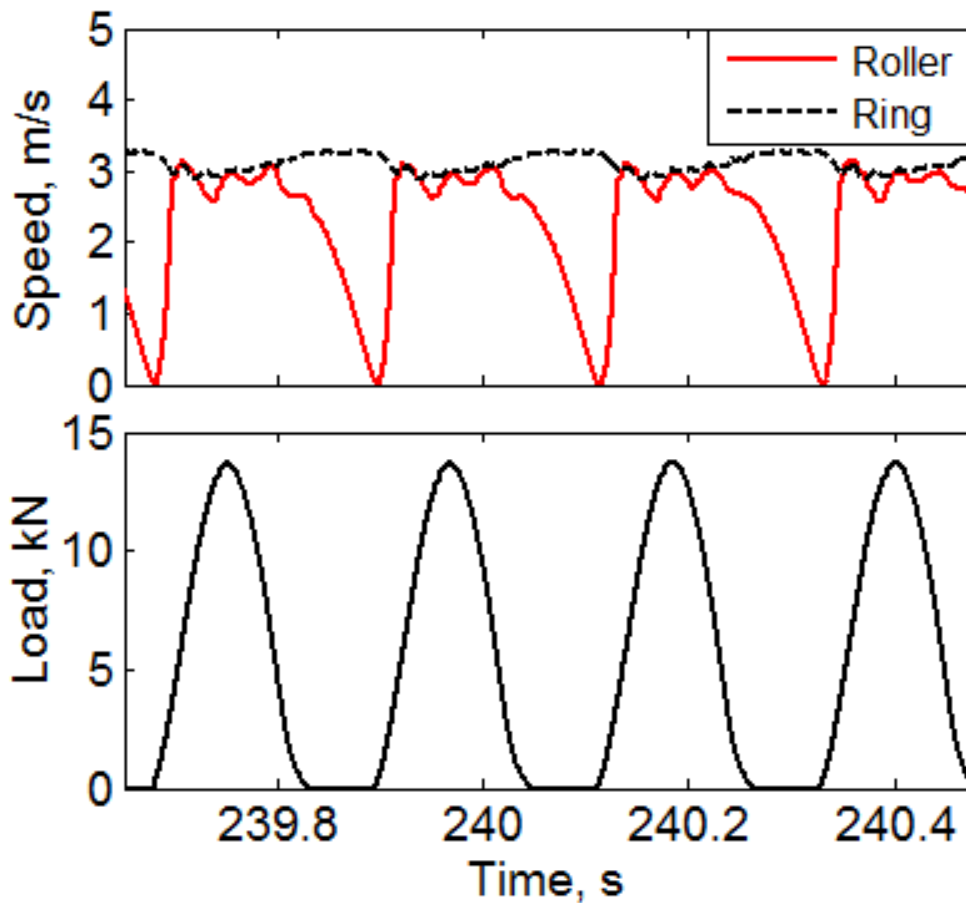
Figure 4: Typical set of recorded data showing time histories of contact load, roller speed and raceway speed for 4 loading cycles. The roller enters the loading phase at zero speed, accelerates to the velocity of the driving raceways during early stages of the loading phase, is nominally in pure rolling for the remainder of the loaded zone and is braked back to zero speed during the unloaded phase. The recorded kinematics simulate the passage of a rolling element through loaded and unloaded zones of a rolling bearing that is experiencing sliding between elements and raceways. (Note: the raceway speed is set to a constant value and the slight deviations from this value that are evident in the figure are due to variations in driving motor torque due to transient load)
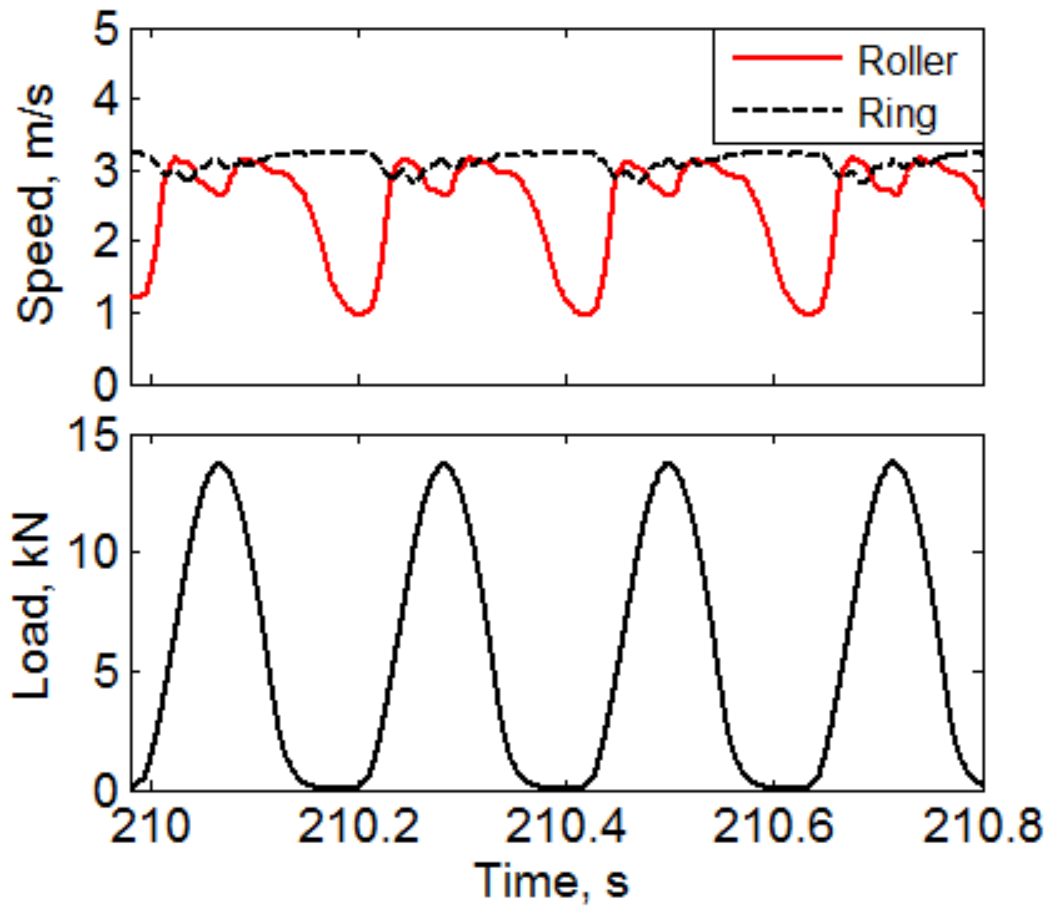
Figure 5: Example of recorded load and speed data for the case when the roller does not lose all of its rotational speed in the unloaded phase and re-enters the loading zone with a non-zero speed.
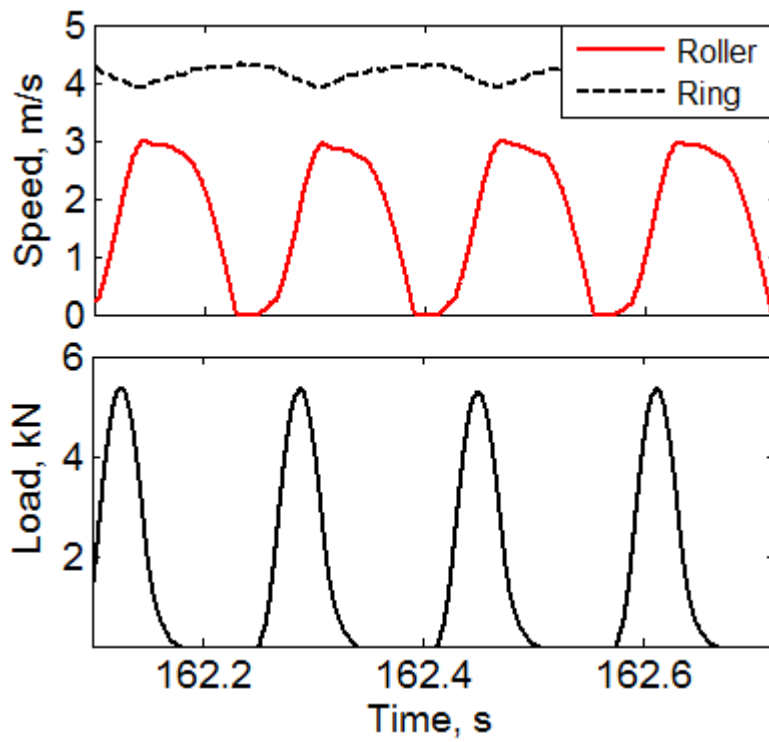
Figure 6: Example of recorded load and speed data for the case when the test roller does not accelerate fully to the speed of the driven raceways during the loading zone so that sliding persists throughout the loaded zone.
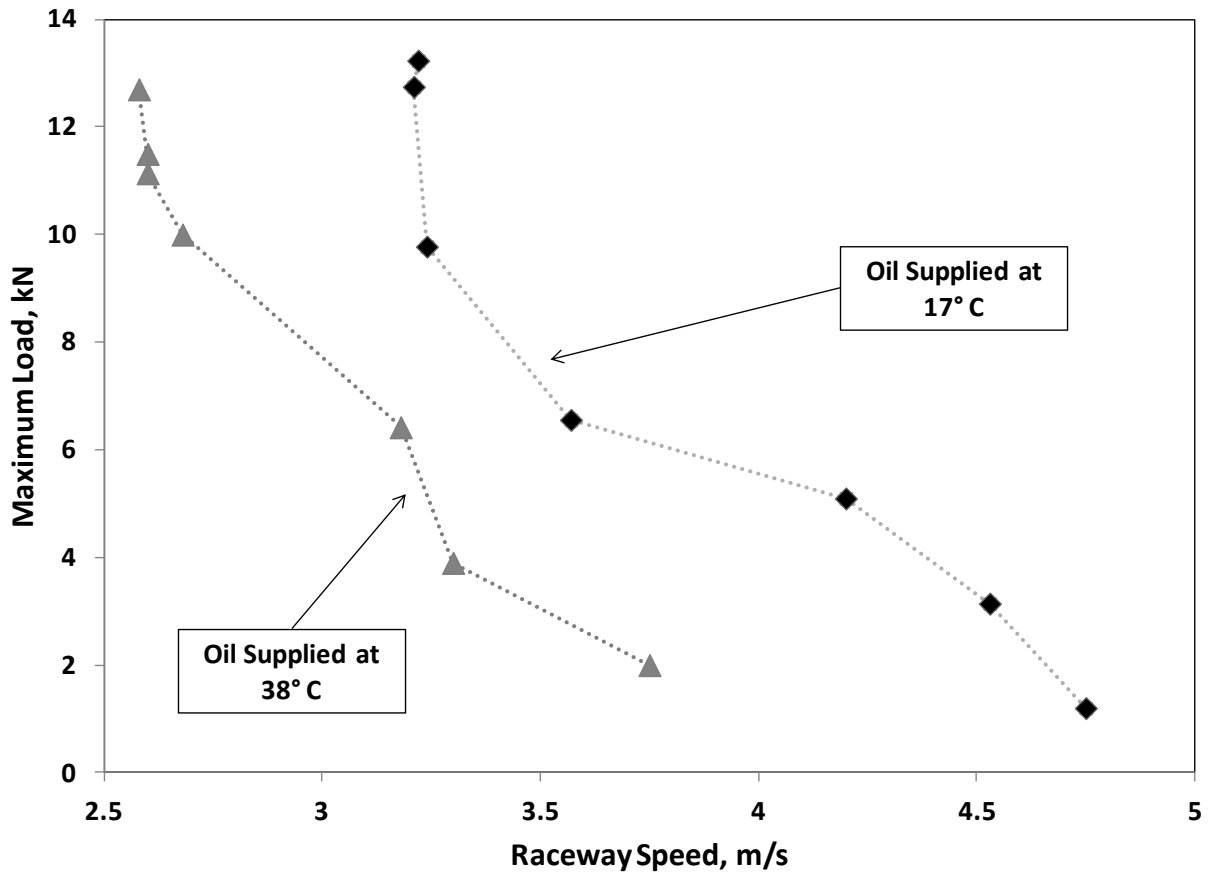
Figure 7: Plot of maximum applied cycle load (P_{max}) against raceway speed (V) at which smearing was recorded for oil supply temperatures of 17°C and 38°C .
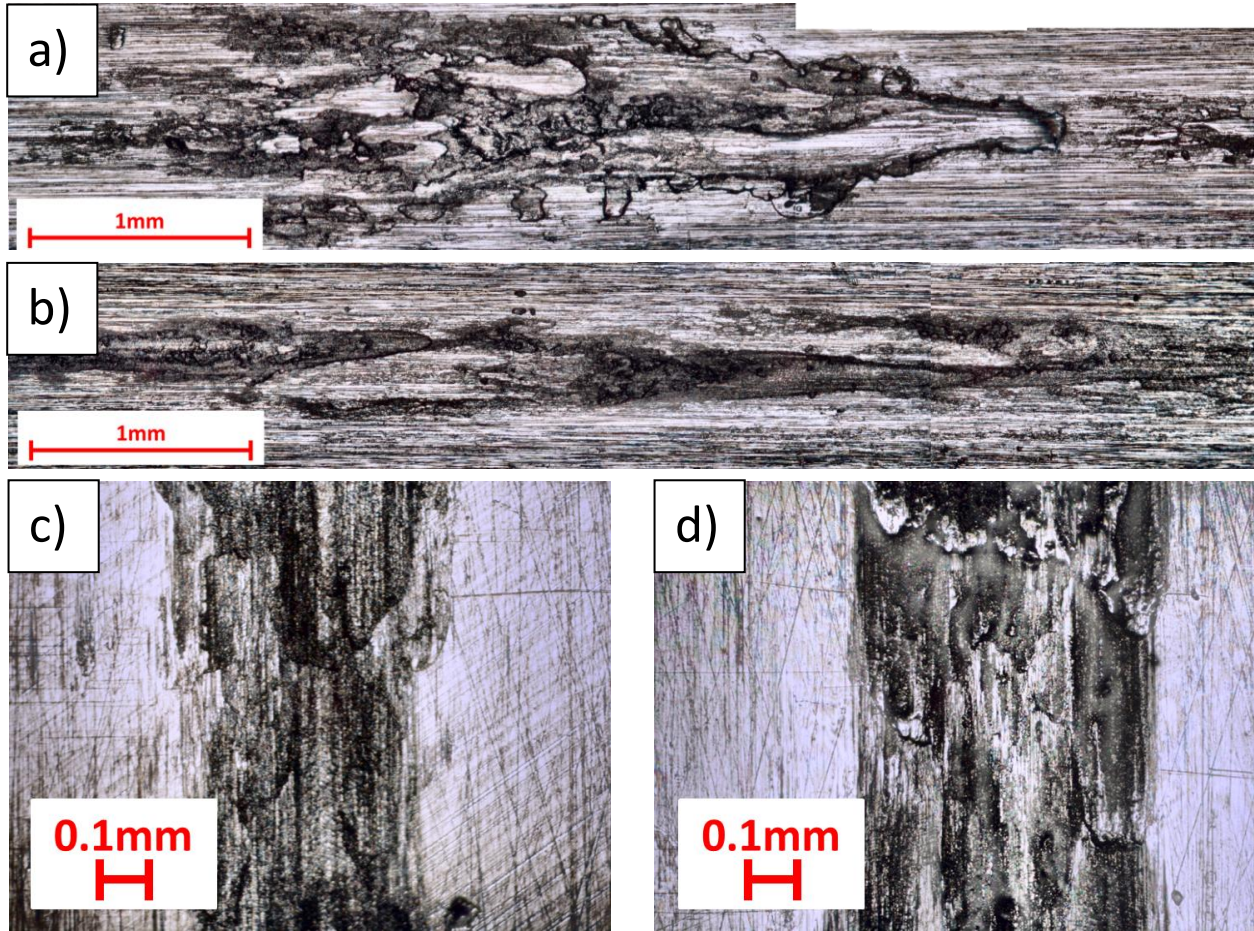
Figure 8: High dynamic range (HDR) images of smearing damage on specimens from Test 7 in Table 2 (P_{max} =13.23 kN, V = 3.22 m/s): a) the very start of the smearing mark on lower raceway, b) smearing on upper raceway, (c) and (d) smeared track on roller at two different positions

Figure 9: A high dynamic range (HDR) image of the very start of the smearing mark on the

lower raceway from Test 2 in Table 2 (P_{max} = 3.14 kN, V = 4.53 m/s)
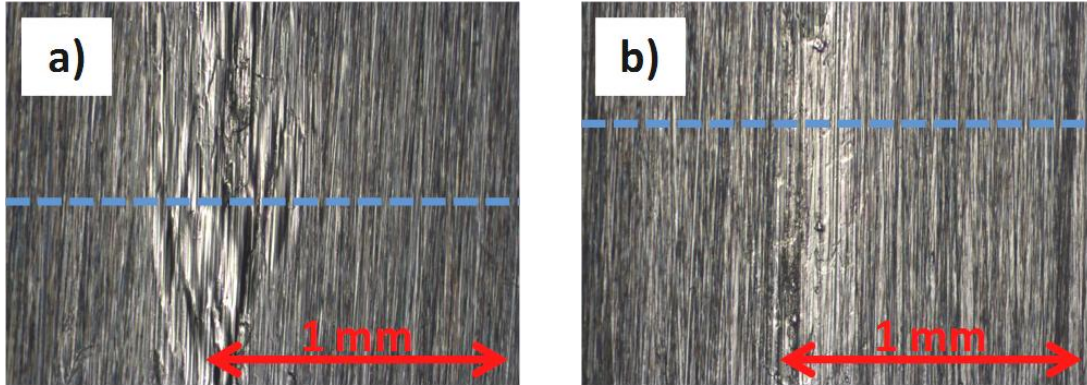
Figure 10: Example images of the smearing scar on the lower disc specimen from Test 6: a) relatively heavily damaged area, b) an area with relatively light damage. The blue broken line indicates the general position where the respective roughness profiles shown in Figure 11 were taken.
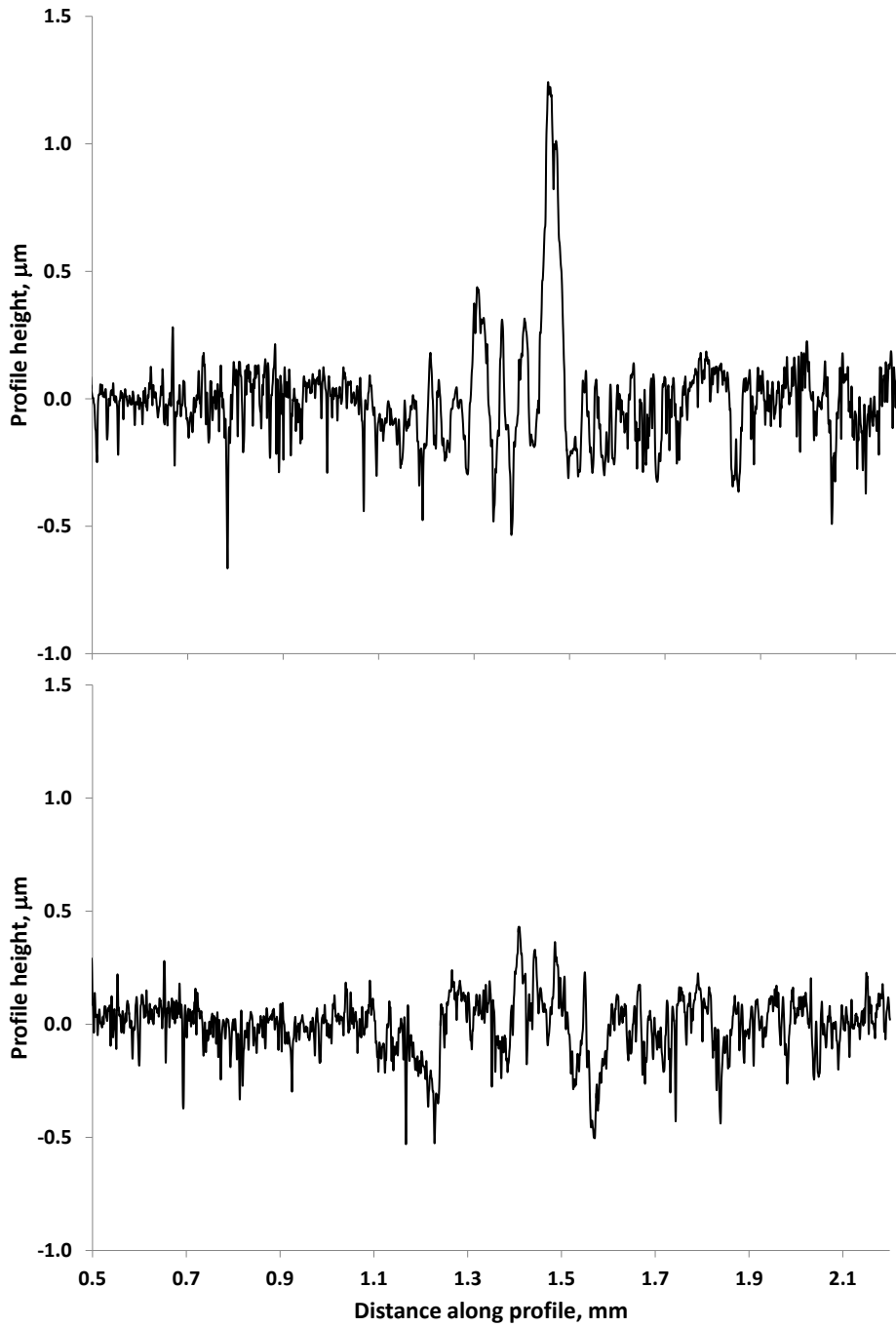
Figure 11: Example surface profiles of the damaged area on the lower raceway specimen of Test 6. Lower plot is a profile of the relatively less damaged area and upper of the visibly more damaged area.
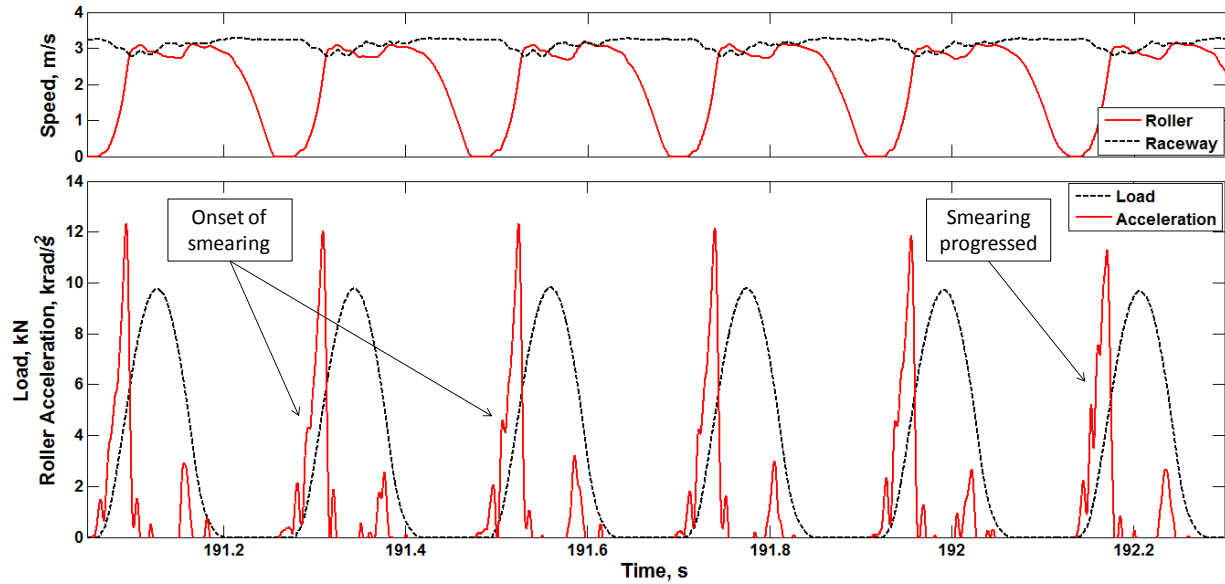
Figure 12: Recorded time histories of load, roller acceleration, roller speed and raceway speed over 6 loading cycles from Test 5 showing the first onset of smearing damage – the 1st cycle shown has a smooth acceleration trace as the roller is accelerated through the lubricant shear stress only, the 2nd cycle shows the first irregularity in the acceleration trace indicating first metal-to-metal contact, the spikes in roller acceleration then grow indicating damage progression.
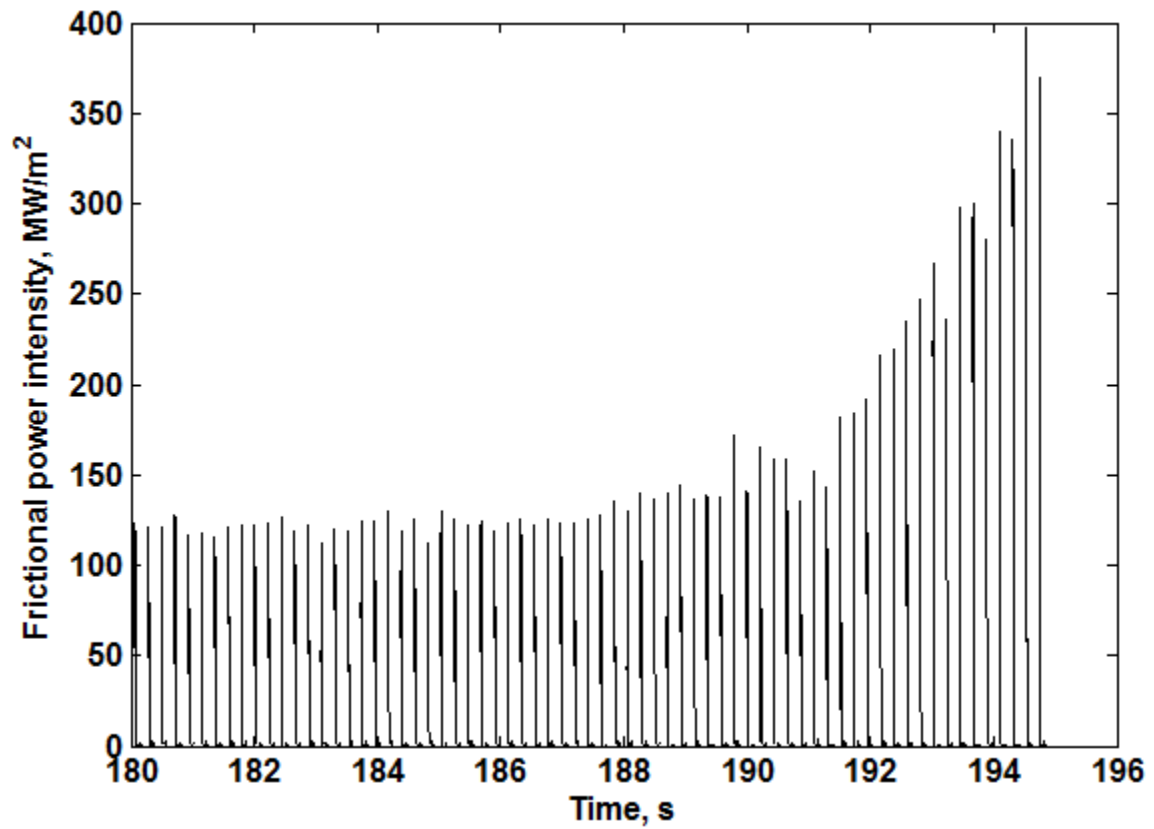
Figure 13: Plot of instantaneous frictional power intensity (FPI) against test time spanning the onset of smearing for Test 5 (the same test as shown in Figure 12 above). Prior to initiation of smearing damage maximum FPI is constant at each loading cycle but increases rapidly once smearing has occurred.
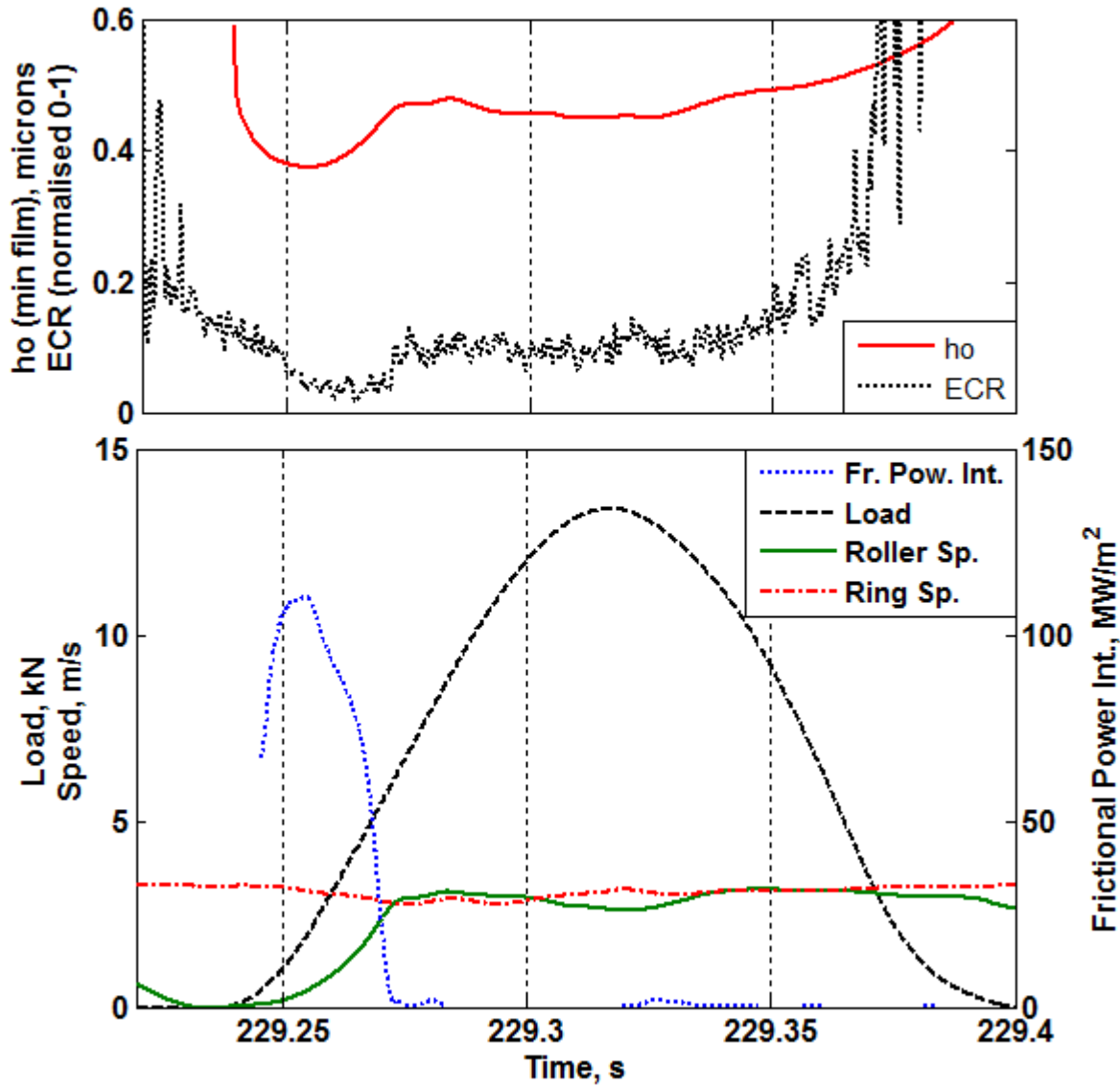
Figure 14: Recorded data for a single loading cycle just prior to occurrence of smearing in Test 7. Load, speed and electrical contact resistance data is as recorded during the test. Frictional power intensity is calculated using Equation 4 and film thickness values are calculated using Dawson and Hamrock EHL equation [26] with recorded speeds and loads and oil viscosity at supply temperature ($17\,^{0}$C).
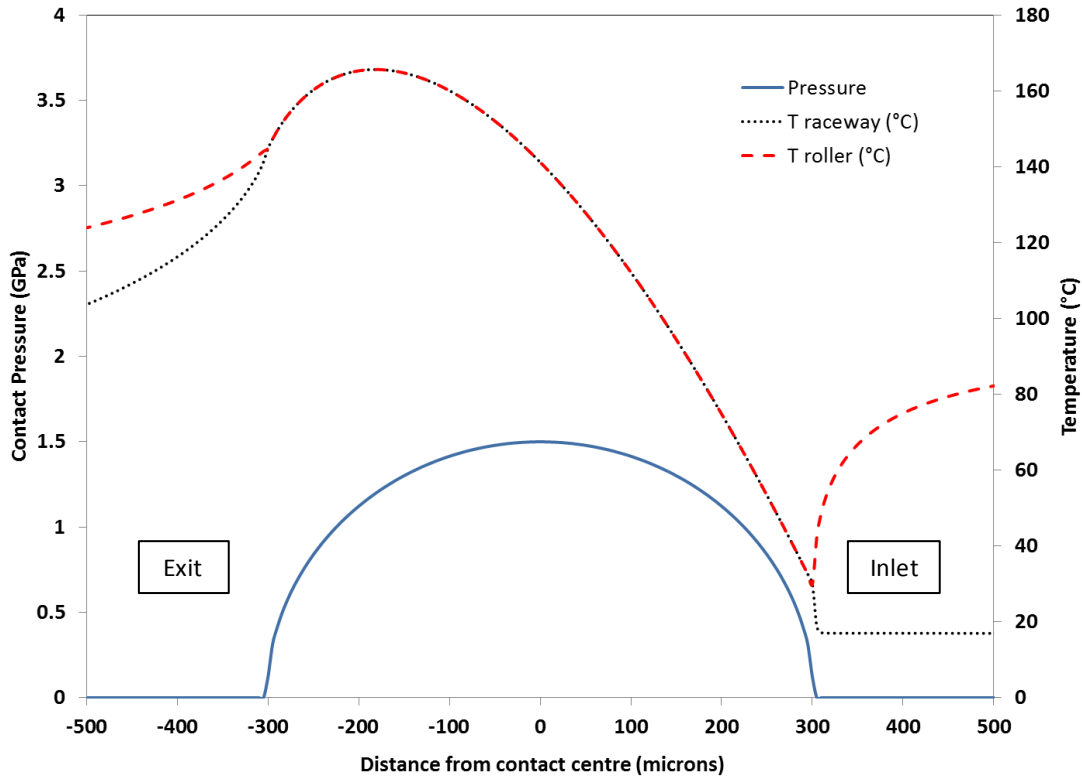
Figure 15: An example of estimated contact temperature distribution for the test roller-raceway contact obtained using the steady state, two-dimensional thermo-mechanical model from [27]. Smooth, dry, steady-state, line contact approximation; details explained in the test. Contact conditions as recorded for Test No. 2: $\ddot{q}$ = 130 MW/m^2, V_s = 4.53 m/s (V_{ring} = 4.53 m/s, V_{roller} = 0 m/s), bulk temperature = 17°C, Load = 0.71 N/μm (set so that the contact width and maximum pressure in this line contact approximation with steady load are equal to those at the instant of maximum FPI in the test elliptical contact with transient load); Material properties of ring and roller are those of bearing steel: k = 45 W/mK, C = 460 J/KgK, density = 7860 kg/m^3, E= 207 GPa, υ = 0.3.
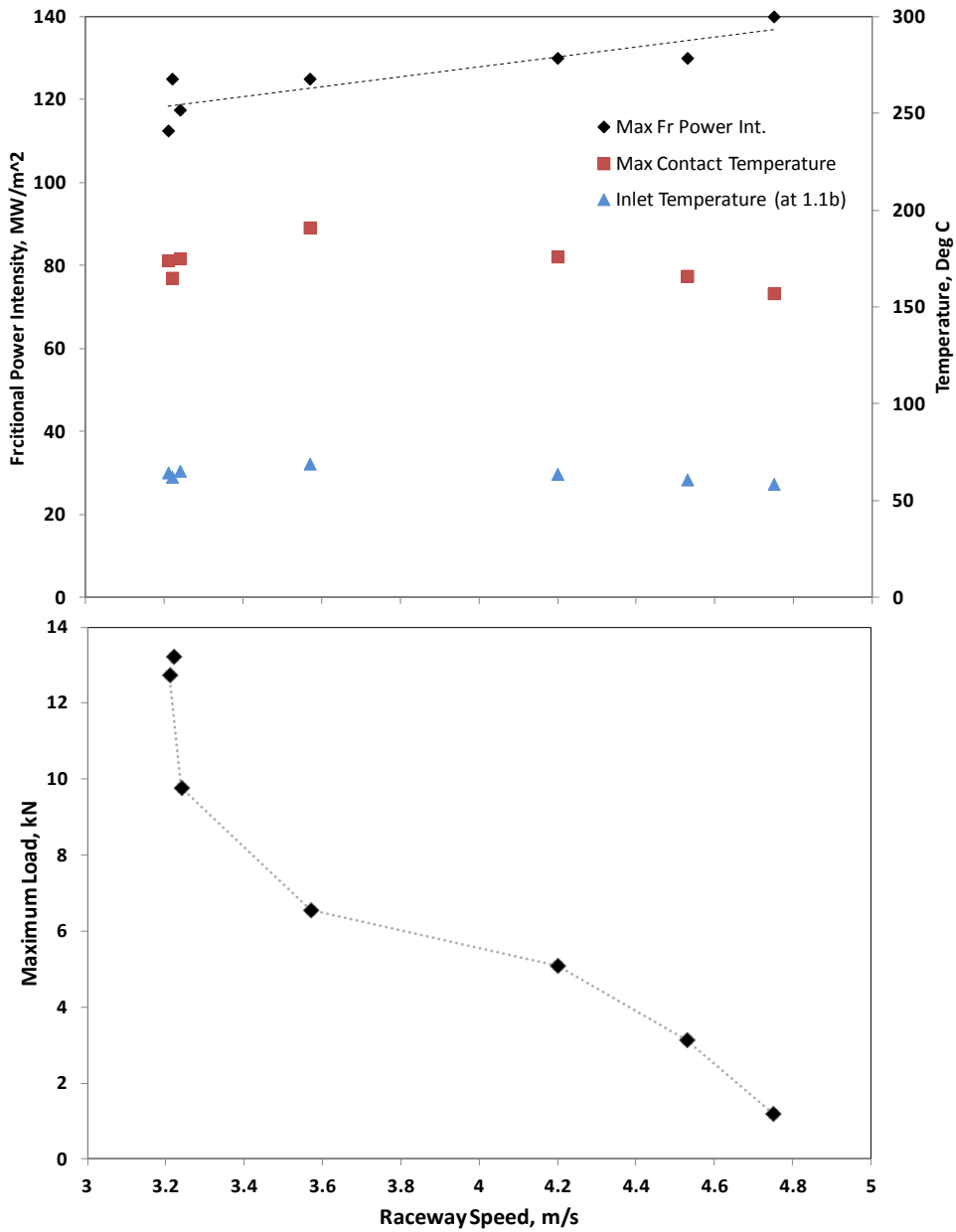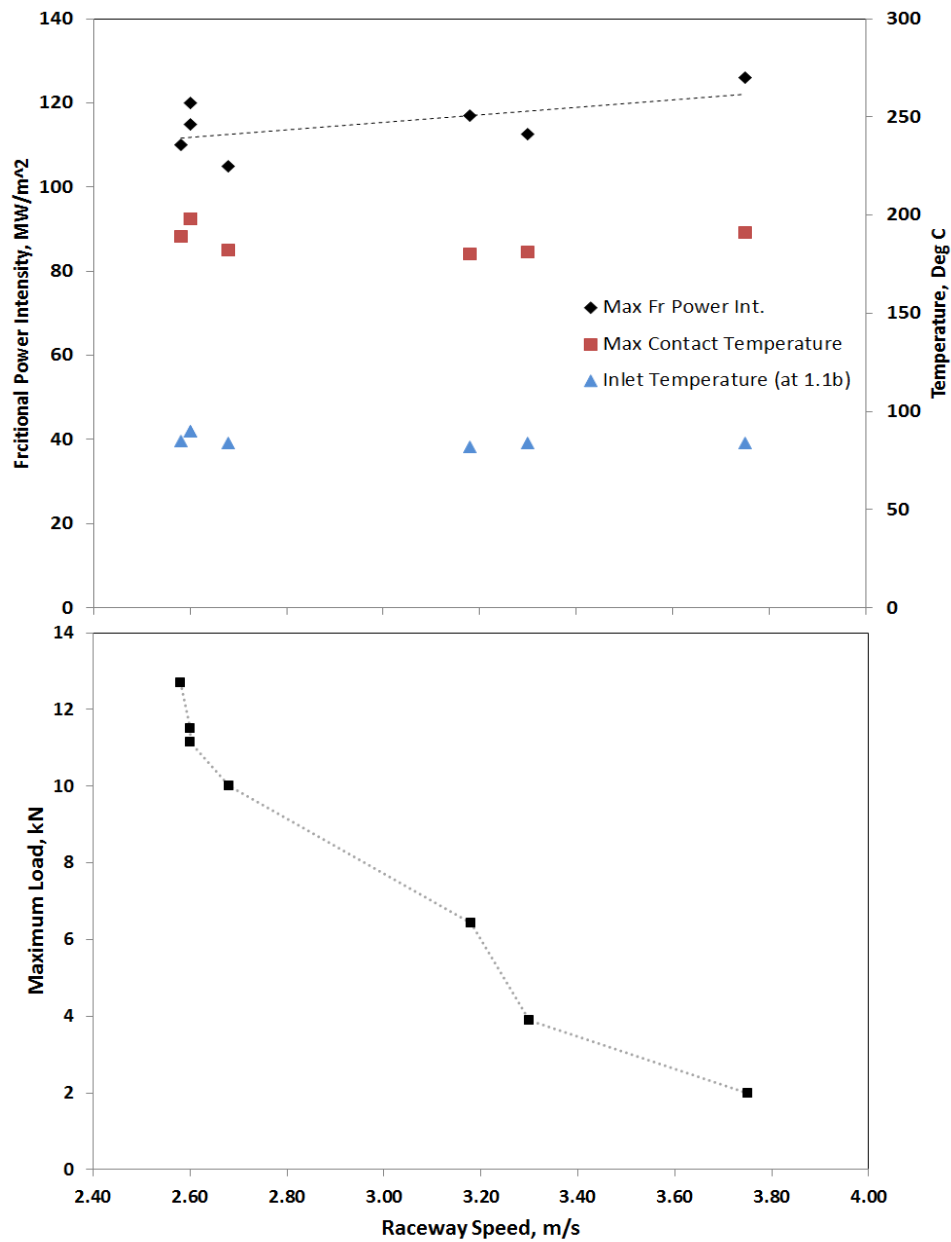
Figure 16: Plot of maximum frictional power intensity and predicted maximum contact temperatures and inlet temperatures (at position 0.1*b from contact edge) against raceway speed at which smearing occurred in tests at oil supply temperature of 17° C. The lower graph shows the corresponding maximum applied load for each test.

Figure 17: Plot of maximum frictional power intensity and predicted maximum contact temperatures and inlet temperatures (at position 0.1*b from contact edge) against raceway speed at which smearing occurred in tests at oil supply temperature of 38° C. The lower graph shows the corresponding maximum applied load for each test.
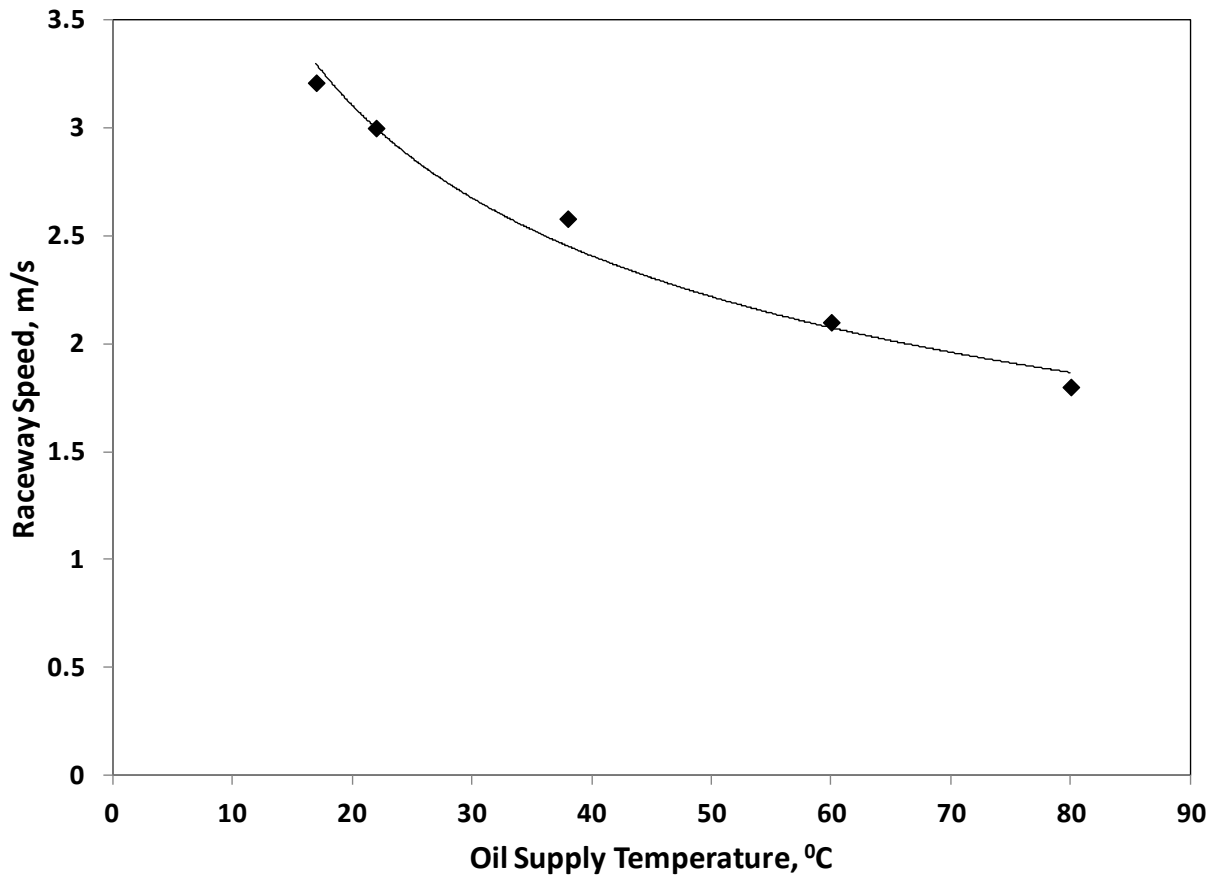
Figure 18: Plot of raceway speed (V) at which smearing occurred against oil supply temperature (T_{sup}). Tests at constant maximum load of 12.75 kN ($p_0 = 3.2$ GPa).